Sequence boundaries are impedance contrasts: Core-seismic-log integration of Oligocene–Miocene sequences, New Jersey shallow shelf

Kenneth G. Miller[1], James V. Browning[1], Gregory S. Mountain[1], Maria A. Bassetti[2], Donald Monteverde[1,3], Miriam E. Katz[4], Jenny Inwood[5], Johanna Lofi[6], and Jean-Noel Proust[7]

[1]*Department of Earth and Planetary Sciences, Rutgers University, Piscataway, New Jersey 08854, USA*
[2]*Laboratoire CEFREM Bat U, University of Perpignan, 52 Avenue Paul Alduy, Perpignan, 66860, France*
[3]*New Jersey Geological Survey, PO Box 427, Trenton, New Jersey 07640, USA*
[4]*Department of Earth & Environmental Sciences, Rensselaer Polytechnic Institute, Troy, New York 12180, USA*
[5]*Department of Geology, University Road, University of Leicester, Leicester LE1 7RH, UK*
[6]*Geosciences Montpellier CC 60, Université Montpellier 2 – 34095, Montpellier Cedex 5, France*
[7]*Géosciences, CNRS, Université Rennes, Campus de Beaulieu, 35042 Rennes, France*

ABSTRACT

Integrated Ocean Drilling Program Expedition 313 continuously cored uppermost Eocene to Miocene sequences on the New Jersey shallow shelf (Sites M27, M28, and M29). Previously, 15 Miocene (ca. 23–13 Ma) seismic sequence boundaries were recognized on several generations of multichannel seismic profiles using criteria of onlap, downlap, erosional truncation, and toplap. We independently recognize sequence boundaries in the cores and logs based on an integrated study of core surfaces, lithostratigraphy and process sedimentology (grain size, mineralogy, facies, and paleoenvironments), facies successions, stacking patterns, benthic foraminiferal water depths, downhole logs, core gamma logs, and chronostratigraphic ages. We use a velocity-depth function to predict the depths of seismic sequence boundaries that were tested by comparison with major core surfaces, downhole and core logs, and synthetic seismograms. Using sonic velocity (core and downhole), core density, and synthetic seismograms, we show that sequence boundaries correspond with acoustic impedance contrasts, although other stratal surfaces (e.g., maximum flooding and transgressive surfaces) also produce reflections. Core data are sufficient to link seismic sequence boundaries to impedance contrasts in 9 of 12 instances at Site M27, 6 of 11 instances at Site M28, and 8 of 14 instances at Site M29. Oligocene sequences have minimal lithologic and seismic expression due to deep-water locations on clinoform bottomsets. Miocene sequences (ca. 23–13 Ma) were sampled across several unconformity clinothems (prograding units) on topset, foreset, and bottomset locations. Excellent recovery allows core-seismic integration that confirms the hypothesis that unconformities are a primary source of impedance contrasts. Our core-seismic-log correlations predict that key seismic surfaces observed in other subsurface investigations without core and/or well logs are stratal surfaces with sequence stratigraphic significance.

INTRODUCTION

The field of stratigraphy was revolutionized by the realization that seismic profiles image unconformity-bounded units and that these units, termed sequences, are the fundamental building blocks of the stratigraphic record (Vail et al., 1977; Mitchum et al., 1977; see historical overviews in Nystuen, 1998; Embry, 2009). Seismic reflections are caused by abrupt vertical changes in acoustic impedance, the product of a material's density (ρ) and sonic velocity (v). Vertical changes in impedance are expressed by a reflectivity coefficient, R that provides a measure of the amount of seismic energy reflected from an interface:

$$R = (\rho v_1 - \rho_2 v_2)/(\rho_1 v_1 + \rho_2 v_2), \qquad (1)$$

where $\rho_1 v_1$ and $\rho_2 v_2$ are the acoustic impedance of layer 1 overlying layer 2, respectively. A seismic reflection results from the convolution of an impedance contrast with a seismic source signal assumed to be a wavelet traveling perpendicular to the change in impedance; the larger the value of R, the more energy reflected. Sharp vertical changes in impedance yield large R values and cause strong seismic reflections. However, any of several circumstances (e.g., graded bedding) can cause gradual vertical changes in impedance and corresponding gradual vertical changes in R. These gradual changes will tend to reflect less seismic energy than narrowly defined, more abrupt changes in impedance.

A prevalent misconception was that lithologic variations (either lateral or vertical) were the primary source of impedance contrasts and seismic reflections, until studies at Exxon Production Research Company (Exxon herein) suggested that abrupt impedance contrasts produced at stratal surfaces (including unconformities) were the primary source of seismic reflections (see discussion in Vail et al., 1980). Because unconformable surfaces (versus lateral changes in facies) divide a succession of sediments into chronostratigraphic units, this implied that seismic profiles could track geologic history in time and space. This breakthrough resulted in the field of seismic stratigraphy, with the sequence boundary as the fundamental surface (Mitchum et al., 1977).

Mitchum et al. (1977, p. 53) defined a depositional sequence as a "stratigraphic unit composed of a relatively conformable succession of genetically related strata and bounded at its top and base by unconformities or their correlative conformities." Two aspects of their definition have been extensively debated: genetically related, implying a global sea-level control, and the correlative conformity, that presumes that there are locations along a sequence where there is no time gap with the underlying sequence. Many view tectonic, not sea-level, changes as the genetic control (e.g., Catuneanu, 2006; Embry, 2009), though it is generally agreed that

Geosphere; October 2013; v. 9; no. 5; p. 1257–1285; doi:10.1130/GES00858.1; 17 figures; 1 table; 1 supplemental file; 1 supplemental figure; 1 supplemental table.
Received 8 August 2012 ♦ Revision received 14 June 2013 ♦ Accepted 1 July 2013 ♦ Published online 14 August 2013

unconformities are associated with the lowering of base level due to eustatic and/or tectonic influences, with sediment supply having minimal influence on formation of sequence boundaries (Christie-Blick, 1991; Christie-Blick and Driscoll, 1995). The concept of a correlative conformity may be applicable in deep-sea pelagic sections, but its applicability in shallow shelf strata, where there are generally "more gaps than record" (Ager, 1973, p. 28), remains to be proven. Despite debates about definitions, unconformities provide a fundamental means for objectively subdividing the stratigraphic record.

Seismic sequence boundaries are objectively recognized by certain stratal geometries: onlap, erosional truncation, toplap, and downlap (although downlap surfaces are also associated with maximum flooding surfaces, MFS; Vail et al., 1977). Seismic sequence stratigraphy is limited by vertical resolution (Widess, 1973; typically 15–25 m in older generation data, 5 m in modern multichannel seismic profiles using air guns, and higher resolution with higher frequency sound sources), horizontal resolution (Sheriff, 1985), seismic artifacts (Tucker and Yorston, 1973), and the fact that lithology must be inferred. Inferences of lithology from seismic profiles still remain highly speculative, although three-dimensional (3-D) data sets improve such predictions based on seismic geomorphology and mapping of architectural elements (e.g., Deptuck et al., 2007).

Depositional sequences can also be recognized in outcrops, coreholes, and well logs (e.g., Van Wagoner et al., 1990), providing finer vertical resolution and a direct link of sedimentary facies to sequences. Sequence-bounding unconformities are recognized in outcrops and coreholes on the basis of physical stratigraphy, including irregular contacts, rip-up clasts, other evidence of reworking, heavy bioturbation, major facies changes, and stacking pattern changes (e.g., changes in coarsening versus fining upward). Unconformities, including paraconformities with no obvious surface of erosion, can be inferred from age breaks (hiatuses). Sequences in logs can be recognized by stacking patterns, particularly of parasequences (those bounded by flooding surfaces; Van Wagoner et al., 1990), and large upsection gamma-log increases associated with sequence boundaries, although these also occur at MFS.

Using seismic profiles, Exxon developed a cycle chart based on sequence-bounding unconformities observed around the world (Vail et al., 1977). Because these unconformities were interpreted as interregional, they were attributed to a global process: sea-level falls. They also ascribed patterns of onlap to sea-level rise and used these to create a global sea-level curve by measuring sea-level rises from the vertical component of onlap (coastal encroachment) and falls from downward shifts in coastal onlap. On the Vail curve (Vail et al., 1977), sea-level falls were shown as virtually instantaneous. Thorne and Watts (1984) showed that this saw-toothed pattern with extremely rapid falls was an artifact. The next generation Exxon sea-level curve (the Haq curve; Haq et al., 1987) also did not fully account for the effects of subsidence (thermal and differential local), compaction, and flexural loading (Christie-Blick et al., 1990). The Haq et al. (1987) eustatic estimate was obtained as follows (see summary in Miller et al., 2011): (1) the relative sea-level curves obtained from various basins were scaled to Pitman's (1978) long-term (10^7 yr) sea-level estimate of ~250 m above present ca. 80 Ma; (2) elevations of flooding surfaces were scaled so that those on the million year scale reached the envelope of the long-term curve; and (3) lowstands were chosen to not exceed the depths of Pleistocene sea-level falls except during the middle Oligocene. Greenlee and Moore (1988) attempted to correct for subsidence, loading, and compaction effects in the Exxon curves, but showed that any such attempt was critically dependent on the assumption of the water depth at the lowest point of onlap. Determining the depositional environment (nonmarine, shallow marine, or deep marine) of this lowest point of onlap is an objective addressed by Integrated Ocean Drilling Program (IODP) Expedition 313 (Mountain et al., 2010). Empirical comparisons of the Exxon amplitudes (Vail et al., 1977; Haq et al., 1987) with other records (e.g., Sahagian et al., 1996; Miller et al., 2005; John et al., 2004, 2011) show that the former are too high by more than a factor of 2.

The work of Exxon was groundbreaking, but the assumptions made require testing, including the assumption that sequence boundaries are a primary cause of impedance contrasts. The Ocean Drilling Program (ODP) and its successor (IODP) identified as high-priority objectives (1) determining the history of sea-level changes and (2) evaluating the processes governing the responses of margin sedimentation patterns to sea-level change. The continental margin of New Jersey was one of the first targeted by the ODP and IODP for seismic profiling, coring, and logging to address these objectives.

The New Jersey passive continental margin (Fig. 1) provides a natural laboratory for evaluating sequences and sea level because of tectonic stability, thick Miocene sediments, and abundant seismic, well log, and well data for planning drilling (summaries in Miller et al., 1997a, 2005, 2011; Mountain et al., 2010). Tectonism in New Jersey has been dominated by passive effects, including simple thermoflexural subsidence and Airy loading (Kominz et al., 1998, 2002), although glacial isostatic adjustments complicate the Pliocene and younger record (e.g., Peltier, 1998; Raymo et al., 2011). Evidence of faulting is lacking in the Miocene offshore section except for compaction faults (e.g., between 600 and 1000 m seaward of common depth point, cdp 3000; Fig. 2; Figs. S32 and S33 in the Supplemental File[1]). However, there is evidence of differential subsidence between Miocene strata in New Jersey and Delaware (Browning et al., 2006) and recent studies have suggested that the stratigraphic record of this region was overprinted by changes in mantle dynamic topography (Moucha et al., 2008; Rowley et al., 2013). Nevertheless, the correspondence between sequence boundaries and global $\delta^{18}O$ increases indicative of ice growth (Miller et al., 1998, 2005; Browning et al., 2013) argues that tectonism does not completely overprint the sea-level signal.

The New Jersey Margin also affords excellent Oligocene–Miocene chronostratigraphic control using integrated biostratigraphy and Sr isotope stratigraphy, as documented for the onshore coastal plain and continental slope sections drilled by ODP Legs 150X and 150, respectively (e.g., Miller et al., 1998) although many slope sections have undergone diagenetic dissolution of carbonate microfossils (Miller et al., 1996b, 1997a; Pekar et al., 1997; Browning et al., 2013). Magnetostratigraphy is generally limited to fine-grained facies and the magnetic signal in shelf sections is overprinted by the growth of greigite (Mountain et al., 2010). Despite these limitations, it has been demonstrated (Browning et al., 2013) that a firm chronology (± 0.25–0.5 m.y.) can be established even in the shallow shelf strata sampled by Expedition 313.

Greenlee et al. (1992) used industry seismic data and wells on the New Jersey continental shelf to illustrate Oligocene–Miocene prograding clinothems, packages of sediment generated by strata that gently prograde seaward into deeper water, bounded by surfaces (in this case sequence boundaries) with distinct sigmoidal (clinoform) shape and sequences. The New Jersey/Mid-Atlantic Transect was designed as a series of coreholes from the onshore New Jersey coastal plain across the shelf to the continental slope and continental rise (Fig. 1; for a history of the transect, see Miller and Mountain, 1994; Mountain et al., 2010) to sample Oligocene–Miocene sequences across clinothems during a time of large glacioeustatic changes (Miller et al., 1987, 1991).

[1]Supplemental File. PDF file of 31 core photographs illustrating stratal surfaces. If you are viewing the PDF of this paper or reading it offline, please visit http://dx.doi.org/10.1130/GES00858.S1 or the full-text article on www.gsapubs.org to view the Supplemental File.

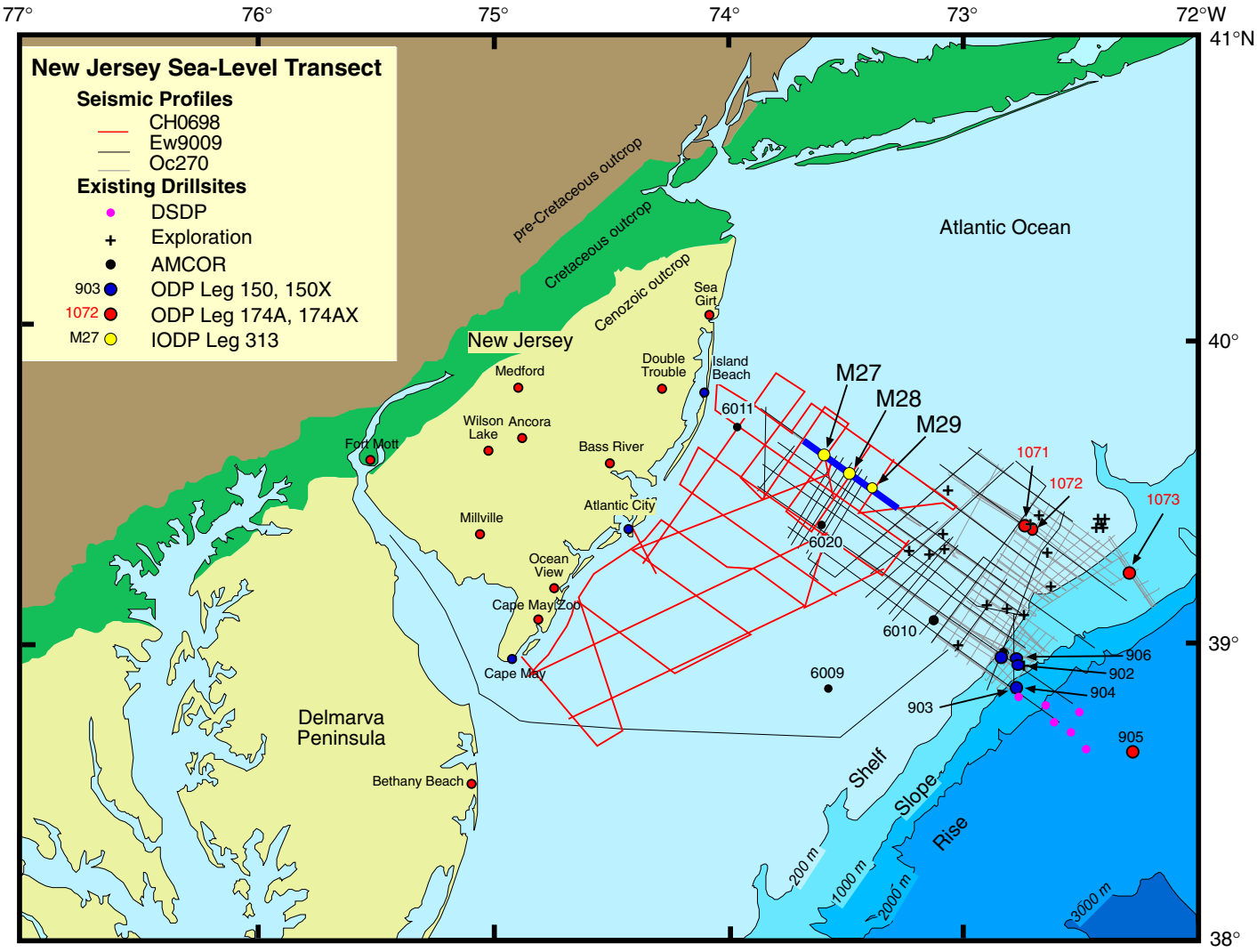

Figure 1. Generalized bathymetric location map of the New Jersey/Mid-Atlantic Margin sea-level transect showing three generations of multichannel seismic data (R/V *Ewing* cruise Ew9009, R/V *Oceanus* cruise Oc270, and R/V *Cape Hatteras* cruise Ch0698), onshore coreholes, and offshore coreholes drilled by the Atlantic Margin Coring Program (AMCOR) (Hathaway et al., 1979), Ocean Drilling Program (ODP), and Integrated Ocean Drilling Program (IODP). Heavy blue line indicates location of Oc270 Line 529 in Fig. 2.

Several locations were targeted in planning a transect that would sample topset, foreset, and bottomset deposits across clinothems (Fig. 2, inset). These include (1) a distal setting (e.g., the continental slope), where the sequence boundaries can be best dated; these were drilled by ODP Leg 150 (Mountain et al., 1994); (2) at the bottomset of each sequence-bounding clinothem (Fig. 2, inset); (3) along the foreset of each clinothem, where the overlying sequence is thickest and strata are physically most complete (i.e., the hypothetical correlative conformity) (Fig. 2, inset); (4) at the topset of each sequence boundary clinothem, immediately landward of the clinoform rollover (Fig. 2, inset); and (5) onshore, where Miocene sequences comprise largely truncated topset deposits (Miller et al., 1997b), although Oligocene sequences sample across clinothems (Pekar et al., 2002). The foreset and topset settings straddle a clinoform rollover where the sedimentary facies and paleodepths may provide a record of water-depth changes across each sequence boundary that is needed to estimate the amplitude of sea-level change (Greenlee and Moore, 1988).

Slope drilling by Leg 150 documented the age and facies of sediments associated with 22 middle Pleistocene to early Eocene seismic reflectors with a temporal resolution of ±0.5 m.y. (Miller et al., 1996b, 1998). In many cases, sequence boundaries on the slope are expressed as the base of slightly coarser grained sediment transported during sea-level lowstands. Leg 174A drilled primarily upper Miocene sequences at outer continental sites on either side of clinoform rollovers, but there was poor recovery in sands (Austin et al., 1998).

Drilling onshore in New Jersey and Delaware by ODP Legs 150X and 174AX sampled Cretaceous to Holocene sequences, also with a temporal resolution of ~±0.5 m.y. (see summary in Miller et al., 1998, 2005). Oligocene to middle Miocene sequence boundaries onshore and on the slope correlate with major $\delta^{18}O$ increases, confirming that they formed during global sea-level lowerings (Miller et al., 1996a, 2005). In addition, the timings of the falls compare well with those of Exxon (Haq et al., 1987), indicating that the cycle chart provides useful information on the timings, although not the amplitudes, of sea-level falls (Miller et al., 2005). As summa-

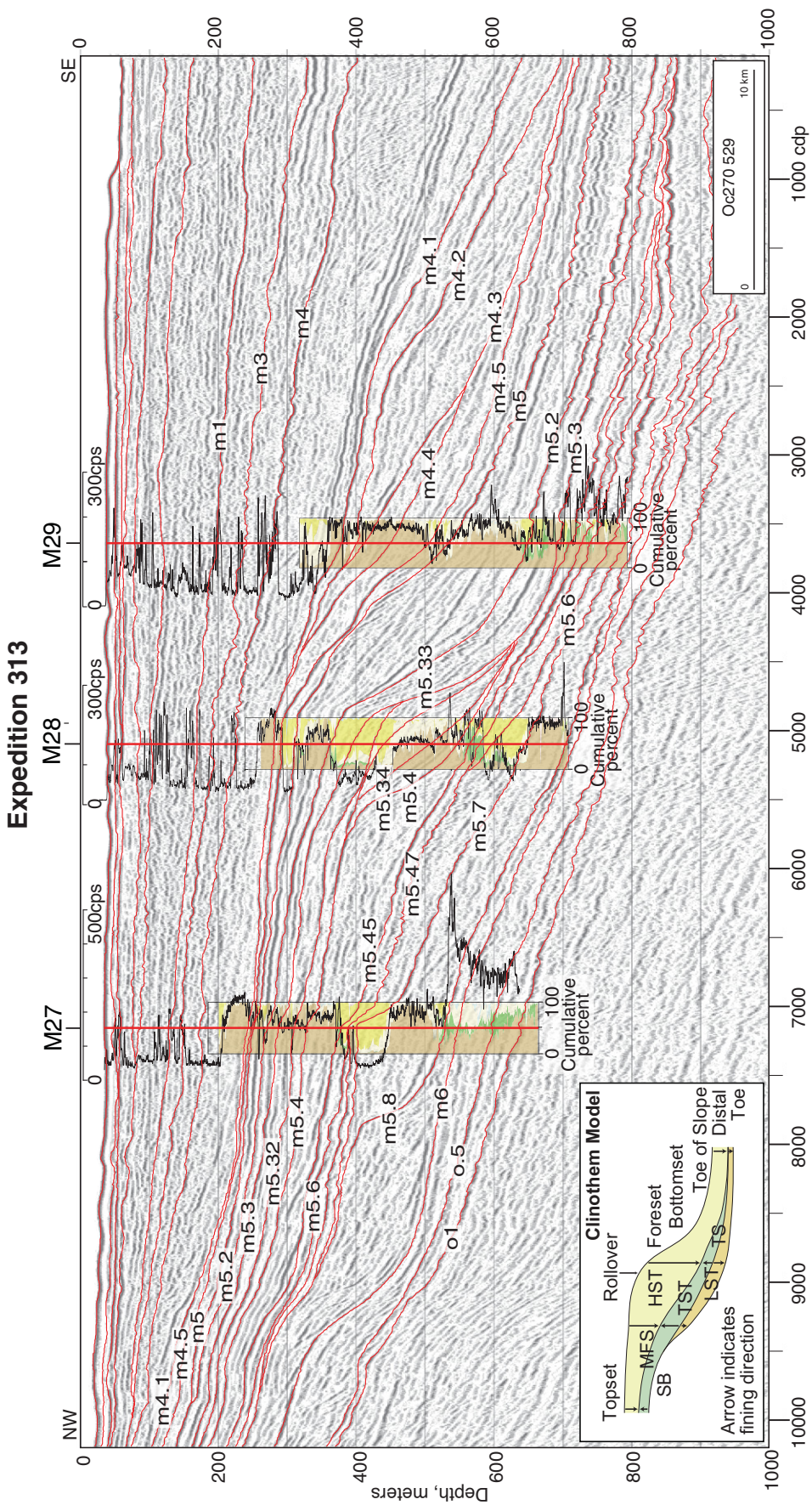

Figure 2. Multichannel seismic profile R/V *Oceanus* cruise Oc270 Line 529 trending northwest to southeast across Integrated Ocean Drilling Program Expedition 313 Sites M27–M29. Traveltime has been converted to depth below sea level (Mountain and Monteverde, 2012). Major seismic sequence boundaries and select intrasequence reflectors (o1, 0.5, m5.34–m5.32) are shown; all others are seismic sequence boundaries (m4.1 is a merged transgressive surface, and sequence boundary in this area). Grain size estimates (in cumulative percent; see Methods discussion in text) and downhole gamma logs (in counts per second, cps) are superimposed at each site location. Inset at lower left is a generalized clinothem model (after Miller et al., 2013b). TS—transgressive surface; TST—transgressive systems tract; LST—lowstand systems tract; HST—highstand systems tract; MFS—maximum flooding surface; SB—sequence boundary. The full-size version of Figure 2 (18 × 26 in) is available at http://dx.doi.org/10.1130/GES00858.S2 or through the full-text article on www.gsapubs.org.

rized in Mountain et al. (2010), previous drilling has (1) provided a chronology of eustatic lowerings for the past 100 m.y. (Miller et al., 1998, 2005); (2) validated the dip transect approach (onshore, shelf, slope) of drilling passive margins for sea-level studies (Mountain et al., 1994, 2010), although the three-dimensionality of sequences requires an additional along-strike component (Fulthorpe and Austin, 2008; Monteverde et al., 2008); (3) shown that unconformities are a source of seismic reflections on the continental slope (Mountain et al., 1994; Miller et al., 1998); and (4) provided a testable record of global sea-level change over the past 100 m.y. (Miller et al., 2005; Kominz et al., 2008), with amplitude estimates of ~20–85 m for million-year-scale variations that agree with oxygen isotopic estimates (Miller et al., 2005, 2011).

Despite the accomplishments of seismic profiling and drilling on the New Jersey Margin, several major goals were not achieved. Because Miocene sequences were sampled far updip on the topsets, they are relatively incomplete and sea-level reconstructions based on them underestimate amplitudes (Miller et al., 2005; Kominz et al., 2008; John et al., 2004). In addition, despite valiant attempts by Leg 174A, the full suite of facies across a clinothem has not been sampled until now. Drilling of the New Jersey shallow shelf by IODP Expedition 313 at Sites M27, M28, and M29 continuously cored and logged Oligocene to Miocene prograding clinothem sequences imaged on multichannel seismic profiles. In this contribution we integrate seismic, core, and log data to provide a firm sequence stratigraphic framework for Oligocene to Miocene sequences on the New Jersey shallow shelf. Pleistocene sequences were discussed in Miller et al. (2013a) and Pliocene strata were not sampled by Expedition 313. We test our correlations with new lithologic, benthic foraminiferal, and age data, and use sonic velocity (core and downhole) and core density data to compute acoustic impedance to provide a robust series of tests of the relationship of sequence boundaries with impedance contrasts.

METHODS

Seismic Interpretation

Several seismic grids obtained on the New Jersey continental shelf and slope (Fig. 1) were used in locating the Expedition 313 sites, building on industry multichannel seismic data (Greenlee et al., 1992).

1. A reconnaissance grid was shot by R/V *Ewing* cruise Ew9009 (Fig. 1) in 1990 across the shelf and slope using a 120 channel, 6 air gun system with ~15 m vertical resolution. This grid imaged additional Oligocene–Miocene prograding clinothem sequences that were not resolvable in the 1975–1977 Exxon multichannel seismic data due to the lower resolution (Greenlee et al., 1992). The Ew9009 multichannel seismic data were used to locate sites drilled on the continental slope by ODP Leg 150 (Mountain et al., 1994; Fig. 1).

2. A higher resolution grid was shot by the R/V *Oceanus* cruise Oc270 in 1995 with 48 channel generator injector gun and HiRes™ (http://www.seismicventures.com/hires.html) equipment with ~5 m vertical resolution. Oc270 Line 529 collected remarkably improved images of features imaged in Ew9009 line 1003 (Fig. 2) across the shelf, although the Oc270 grid focused on the outer continental shelf subsequently drilled by ODP Leg 174A (Austin et al., 1998).

3. Several seismic grids were collected by cruise R/V *Cape Hatteras* cruise CH0698 in 1998 using the same HiRes gear used on Oc270; a regional grid links the middle shelf to onshore New Jersey. Three hazard grids of 150–600 m line spacing were collected to provide detailed control on clinoform geometries, as well as to meet safety guidelines for drilling at Expedition 313 Sites M27, M28, and M29 (Ball et al., 1992).

Together, the 2-D data collected by Oc270 and CH0698 significantly increased the number of sequences resolved (Fig. 2) compared with the earlier Greenlee et al. (1992) and Ew9009 data.

Sites M27, M28, and M29 are located on Oc270 Line 529 (Fig. 2). Analysis of CH0698 seismic profiles built on earlier analyses of Exxon (Greenlee et al., 1992) and Ew9009 and Oc270 profiles (Miller and Mountain, 1994; G.S. Mountain, K.G. Miller, and N. Christie-Blick, our own data) that identified seismic sequence boundaries based on reflector terminations of onlap, downlap, erosional truncation, and toplap. Greenlee et al. (1992) named sequence boundaries by color, from oldest to youngest as pink-3, blue, sand, ochre, green, pink, blue, yellow, and tuscan. These sequence boundaries were changed to an alphanumeric designation (m6, m5.6, m5.4, m5.2, m5, m4, m3, m2, and m1, respectively) to allow for additional sequence boundaries noted in higher resolution Ew9009 data (Mountain et al., 1994). Reflectors m6 to m4 bracket a lower to middle Miocene (Aquitanian to Serravalian) package that was targeted by drilling at Sites M27–M29. Seismic sequence boundaries from the older data sets were traced and loop correlated throughout the CH0698 grid (Monteverde et al., 2008; Monteverde, 2008). Several additional lower Miocene sequence boundaries were identified between these reflectors and named m5.8, m5.7, m5.5, m5.47, m5.45, and m5.3 (Fig. 2; Monteverde et al., 2008; Monteverde, 2008; Mountain et al., 2010). Sequences are named according to their basal reflector boundary, such that sequence m5.2 overlies reflector m5.2.

The stratal significance of reflectors m4.5, m4.4, m4.3, m4.2, and m4.1 (ca. 13.8–12.6 Ma; Fig. 2) have not been firmly determined. Monteverde et al. (2008) first traced these seismic reflections between m5 and m4 just seaward of Site M29, but did not loop correlate or confirm reflector terminations on these surfaces. Mountain et al. (2010) reexamined the data set and recognized that m4.5 and m4.2 display evidence for sequence boundaries. We recognize that m4.4 and m4.3 are probably sequence boundaries based on reflector terminations, and reflector m4.1 is probably a merged transgressive surface and sequence boundary at Site M29.

Sequences, Lithology, and Paleoenvironments in Cores and Core-Seismic Integration

We recognize sequence boundaries in the Expedition 313 cores on the basis of physical stratigraphy and age breaks. Criteria for recognizing sequence bounding unconformities in onshore coreholes (e.g., Browning et al., 2006) that were also applied to Expedition 313 cores include (1) irregular contacts, with several centimeters of relief on a 6.2-cm-diameter core; (2) reworking, including rip-up clasts found above the contact; (3) heavy bioturbation, including burrows filled with overlying material; (4) major lithofacies shifts and changes in stacking patterns; (5) gamma-ray increases on topsets associated with changes from low radioactivity sands below to hotter above sequence boundaries, associated with clays, glauconites, and/or marine omission surfaces (e.g., with high U/Th scavenging); (6) shell lags above the contact; and (7) age breaks indicated by Sr isotopic stratigraphy or biostratigraphy. Lithologic expression of the unconformities is clearest on the topsets (landward of the clinoform rollover), where they typically consist of a coarsening-upward shallow-water succession found below the merged sequence boundary-transgressive surface changing abruptly to deeper water, fining-upward deposits above the contact. Sequence boundaries in the foresets are generally subtle lithologically because they juxtapose coarsening-upward highstand bottomsets below and coarsening-upward lowstand deposits above, although they usually exhibit evidence for erosion (Figs. S4, S14, and S24 in the Supplemental File [see footnote 1]). Sequence boundaries are often obscure on bottomsets

where they are overlain by stacked sediment gravity flow deposits (Mountain et al., 2010).

The onshore science party provided core descriptions and differentiated clay, silt, and various sand fractions visually and on smear slides (Mountain et al., 2010). The lithologic descriptions were synthesized into general lithology columns presented here essentially unchanged from Mountain et al. (2010; presented as "Lithology" in Figs. 3–17 herein). In this study we added quantitative and semiquantitative lithology data (Supplemental Table[2]). We quantitatively measured weight percent mud (<63 μm), very fine and fine sand (63–250 μm), and medium sand and coarser sediment (>250 μm) in washed samples at ~1.5 m intervals. We semiquantitatively estimated the abundance of glauconite, shells, and mica in the sand fraction (>63 μm) by splitting 1727 samples into aliquots and visually estimating percentages on a picking tray (Figs. 3–17). The semiquantitative and quantitative percent data were combined and presented as "Cumulative lithology" in Figures 3–17; these clearly show distinct trends in grain size and mineralogy that complement and extend the lithology columns developed in Mountain et al. (2010). They are particularly useful in showing fining-upward and coarsening-upward trends not readily observable in the descriptive lithology (e.g., Fig. 7).

Lithofacies variations are interpreted based on previous studies of shallow-marine sediments using a wave-dominated shoreline model (summarized in Mountain et al., 2010), recognizing upper shoreface (0–5 m), lower shoreface (5–10 m), shoreface-offshore transition (10–30 m), and offshore (>30 m) environments. Benthic foraminiferal biofacies were reported in Mountain et al. (2010) and in greater detail by Katz et al. (2013). Benthic foraminifera provide additional paleodepth constraints particularly for deeper (>30 m) water following the general paleobathymetric model (Miller et al., 1997b) for coeval onshore New Jersey sections. In general, innermost neritic (<10 m) sediments were barren, *Hanzawaia concentrica*–dominated biofacies are inner neritic (10–25 m), *Nonionella pizarrensis*–dominated biofacies are inner to middle neritic (25–50 m), *Buliminella gracilis*–dominated biofacies are middle neritic (50–80 m), *Uvigerina juncea*–dominated biofacies are middle neritic or deeper (>75 m), and high-diversity, low-dominance assemblages with key indicator taxa (e.g., *Cibicidoides pachyderma*, *Hanzawaia mantaensis*, and *Oridorsalis*) are outer neritic (>100 m; Mountain et al., 2010; Katz et al., 2013). We present both benthic foraminiferal paleodepths and integrated paleodepths obtained by combining lithofacies and biofacies constraints (Figs. 3–17). The integrated paleodepth estimates reconcile minor differences between benthic and lithofacies-derived estimates and are used in one-dimensional backstripping (Kominz et al., 1998). Ages of sequences and hiatuses presented (Figs. 3–17) and discussed here (see Results discussion) are derived by integrating Sr isotopic stratigraphy and biostratigraphy (diatoms, nannofossils, and dinocysts) on age-depth diagrams with a resolution of ±0.25–0.5 m.y. (Browning et al., 2013).

The primary purpose of this paper is to reognize sequence-bounding unconformities (Table 1), although the data presented allow limited recognition of stratal surfaces (MFS, transgressive surface [TS], flooding surfaces [FS]) and systems tracts. We recognize MFS as downlap surfaces seismically. In cores, MFS are recognized by (1) a change in stacking pattern from transgressive (generally fining upward) below to regressive (generally coarsening upward) facies above (inset model Fig. 2); (2) maximum water depths as indicated by benthic and percent planktonic foraminifera; (3) finest grain size; and (4) gamma-log peaks. Both highstand systems tracts (HST) and lowstand systems tracts (LST) show regressive stacking patterns. Transgressive surfaces generally are recognized as erosional contacts at the top of the regressive LST; they are generally merged with sequence boundaries on the topsets. Transgressive systems tracts (TST) generally fine upward. Parasequence boundaries (flooding surfaces) are recognized in LST, TST, and HST. We do not recognize systems tracts on the bottomsets due to the difficulty of resolving their complex stratal relationships with the data presented here. Falling stage systems tracts are recognized seismically (for a discussion, see Miller et al., 2013b).

A velocity versus depth function that provided estimated depths to target reflectors was developed to aid drilling decisions aboard the L/B *Kayd* (see Mountain et al., 2010). Depths to reflectors that were identified as sequence boundaries on the basis of seismic geometry (e.g., Mitchum et al., 1977; Abreu et al., 2010) were compared to stratal surfaces when the cores were split and described. Surfaces in cores close to predicted depths (±5 m) were examined for stratigraphic evidence of sequence boundaries, and where confirmed the intervening depositional sequences were classified on the basis of physical stratigraphy, age, and downhole and core-log data. However, in some cases multiple lithostratigraphic surfaces were encountered within a 10 m interval, and the correlation to any of several nearby seismic sequence boundaries remained uncertain. In these instances, lithostratigraphic character was the defining criterion for the location of sequence boundaries and the tie to the seismic record was left unclear (Mountain et al., 2010).

To address inadequacies of several core-seismic correlations, the velocity-depth function was revised (Mountain and Monteverde, 2012). Recalculated interval velocities increased slightly from those used previously, resulting in depths to reflectors generally 3–9 m greater than in Mountain et al. (2010). The revised seismic-core correlations (Figs. 3–17) have been compared with visual evidence (core descriptions and photographs) and log data (downhole and core) as described in the Results discussion, and the resulting agreement is improved over previous efforts (Mountain et al., 2010). While this updated velocity-depth function (Mountain and Monteverde, 2012) clarifies some ambiguities in placement of sequence boundaries in Mountain et al. (2010), any such method is limited in its ability to resolve predicted depths to better than ~±5 m.

Synthetic seismograms from Sites M27A and M29A (Mountain and Monteverde, 2012) provide a check on our seismic-core correlations. Depths of seismic sequence boundaries predicted by synthetic seismograms are indicated with purple arrows in the figures. Synthetic seismograms were not computed for Site M28 because downhole sonic log data were not collected due to hole conditions. The synthetic seismograms were computed to depth using Seismic Micro-Technology (SMT) software as follows (see Mountain and Monteverde, 2012): (1) impedance values were derived from filtered and edited sonic logs and multispectral core logger (MSCL) density values; (2) reflectivity coefficients were calculated at 1 m intervals and with the velocity-depth function described previously converted to depth at 2 ms increments throughout the interval of interest; (3) a source wavelet was extracted from the average of 3 traces centered on each Expedition 313 corehole (using the crossing Oc270 Line 529; Fig. 2); (4) this wavelet was convolved with the reflectivity coefficients to yield a synthetic seismogram in the time window for which there were both sonic downhole log and MSCL data; (5) the synthetic trace was visually matched to a true-amplitude display of the recorded trace at each drill site; and (6) adjustments to the velocity-depth function were made interactively using the SynPAK utility of SMT to move peaks and troughs of the synthetic seismogram up or down in time to better match their apparent analogs in the recorded data. When a reasonable match was achieved without impos-

[2]Supplemental Table. If you are viewing the PDF of this paper or reading it offline, please visit http://dx.doi.org/10.1130/GES00858.S3 or the full-text article on www.gsapubs.org to view the Supplemental Table.

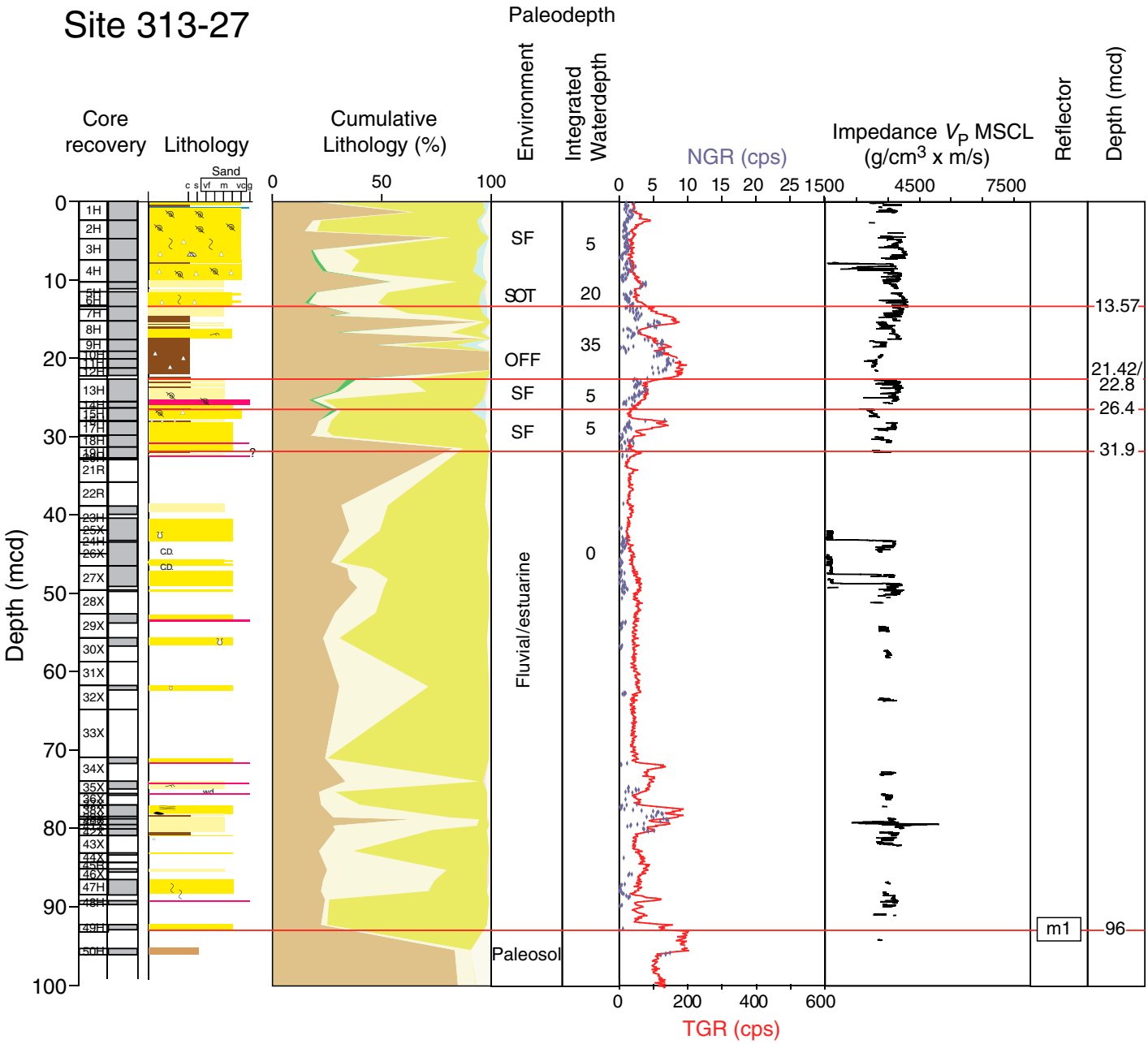

Figure 3 (*explanation and key on following page*). Integrated Ocean Drilling Program Expedition 313 Site M27 sequence m1 and younger Pleistocene sequences (red horizontal line—sequence boundaries), showing core depths in meters composite depth (mcd), core numbers (1H to 21H, where H indicates recovery by hydraulic piston coring, R—rotary, and X—extended core barrel), core recovery (gray—recovered, white—gap), lithology (after Mountain et al., 2010; c—clay; s—silt; vf—very fine sand; m—medium sand; vc—very coarse sand; g—gravel and/or pebbles; symbols in key at bottom), coarse fraction cumulative percent lithology (brown—mud; light yellow—fine quartz sand; dark yellow—medium-coarse quartz sand; green—glauconite sand; blue—carbonate, i.e., shells and foraminifera, and red—mica [see Methods discussion in text]). Environmental interpretation based on lithofacies, integrated water depth in meters based on benthic foraminiferal biofacies and lithofacies, gamma logs (red—downhole as total gamma ray [TGR]; blue dots—MSCL/NGR discrete samples [multispectral core logger/natural gamma ray], scale in counts per second, cps), sonic impedance, reflector (red—sequence boundary, blue—transgressive surface [TS], green—maximum flooding surface), and depths to reflector. (Pleistocene sequences are after Miller et al., 2013b.)

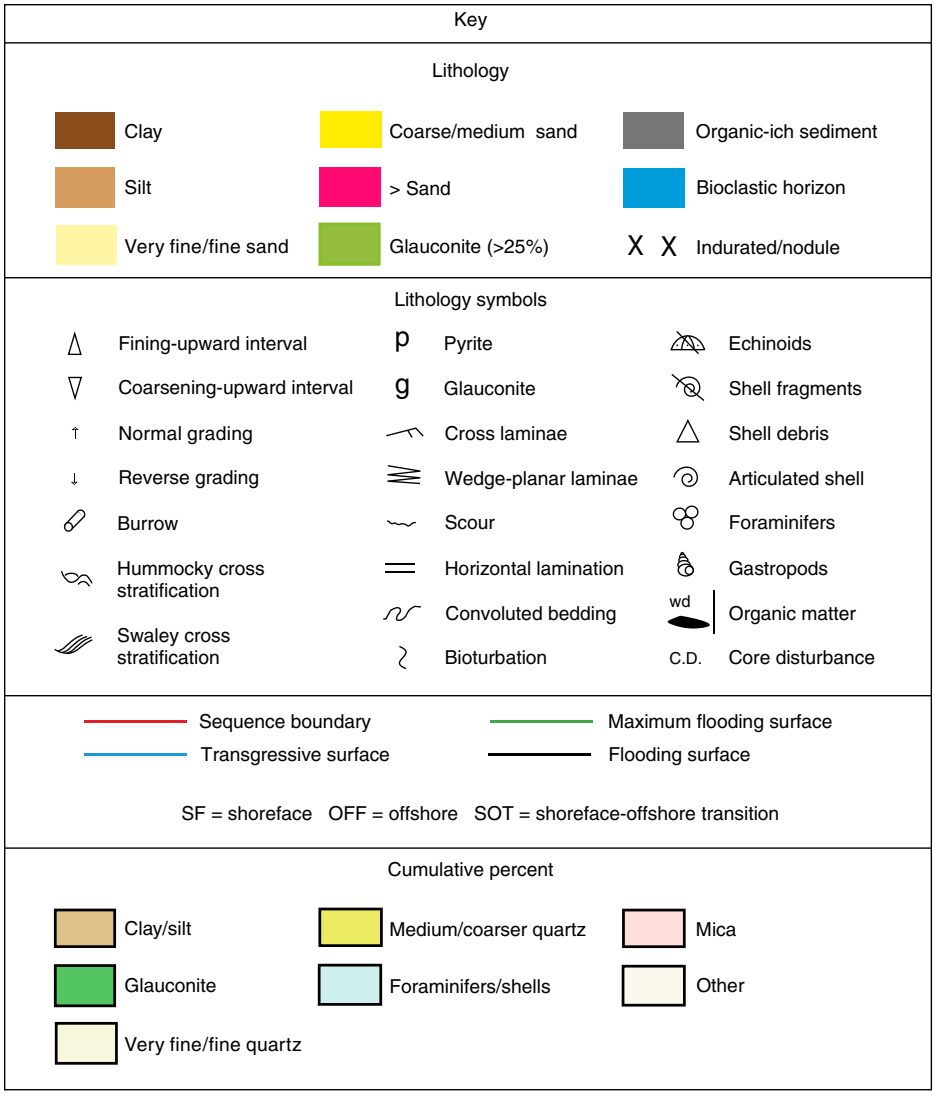

Figure 3 (*explanation and key*).

ing unrealistic velocity-depth values, the synthetic trace was superimposed on a full display of the recorded profile and matching features could then be identified in both seismic traveltime and subseafloor drilling depth.

The SMT SynPAK software convolves a complex synthetic source wavelet with downhole impedance patterns. Success in a synthetic seismogram resembling the actual profile depends on the match of the synthetic source wavelet to the real source. An accurate synthetic wavelet will produce reflections at positions that match the real data, and any acoustic interference patterns caused by closely spaced (e.g., bed to bed) impedance contrasts in the actual profile should also be faithfully reproduced in the synthetic seismogram in terms of position, amplitude, and phase.

Geophysical Log Data

We present gamma-log values obtained downhole through the drill pipe and those obtained by laboratory measurements directly on the core (Figs. 3–17). Gamma-ray measurements on cores confirm the registration of the downhole logs to the core within at least 0.5 m (Mountain et al., 2010). Gamma-log data record lithologic variations primarily of quartz sands versus muds or glauconite-rich sediments, with low gamma readings in sands, high gamma-log values in muds, and generally highest values in glauconite-rich sediments.

Expedition 313 acquired compressional wave (P-wave) velocity data from downhole sonic logs and laboratory measurements on cores. Density measurements were acquired on cores only. Two sets of impedance have thus been calculated using (1) core density and P-wave velocities from cores; and (2) core density and P-wave velocities from sonic logs.

For downhole sonic measurements, the Mount Sopris 2PSA-1000 sonic probe was used to measure P-wave velocities of the formation (15 kHz monopole configuration). The sonic probe is composed of an acoustic transmitter and two receivers. Recorded waveforms were examined and wave arrival times manually selected. We calculated sonic velocity of the rock by measuring the acoustic transit time, knowing the distance between the two receivers (0.3048 m), the velocity in the fluid, and the corehole diameter. At Site M27, downhole sonic logs were acquired in open hole at depths between 192 and 327 m below seafloor (mbsf) and 418 and 622 mbsf. At Site M29, the downhole sonic log covers an interval ranging from 403 to 720 mbsf. In both holes, measurements were acquired at a vertical measurement interval of 10 cm. No sonic logs were acquired at Site M28.

To obtain P-wave velocities on core, an MSCL was used to measure transverse P-wave velocity at a downcore resolution of 1 cm. Two transducers aligned perpendicular to the core axis transmit a P-wave pulse centered on a frequency of 320 kHz horizontally through the core. A pair of displacement transducers monitors the separation between the P-wave transducers to enable correction for small variations of this distance (due to liner diameter variations).

Gamma density was also acquired at a downcore resolution of 1 cm using the MSCL by determining the attenuation of gamma rays (mainly by Compton scattering) that pass through the cores. A small (370 MBq) ^{137}Cs source (half life = 30.2 yr) was used to produce a gamma beam with primary photon energies of 662 keV. The degree of attenuation is proportional to the electron density in the gamma path (Rider, 2006). Gamma attenuation coefficients vary as a function of atomic number, but as most rock-forming minerals have similar and low atomic numbers, the correlation between gamma density and bulk density is generally very good.

The MSCL data are significantly affected by core conditions (e.g., the degree to which the cores fills the liner or presence of cracks) and coring gaps. P-wave velocity data and gamma density have therefore been filtered to omit anomalously low values (<1400 m/s and <1 g/cm^3, respectively). In addition, data affected by end caps were omitted prior to the impedance calculation. To account for the difference in measurement resolution between sonic logs (10 cm) and core densities (1 cm), sonic data were interpolated between successive measurement points. Where the filtering

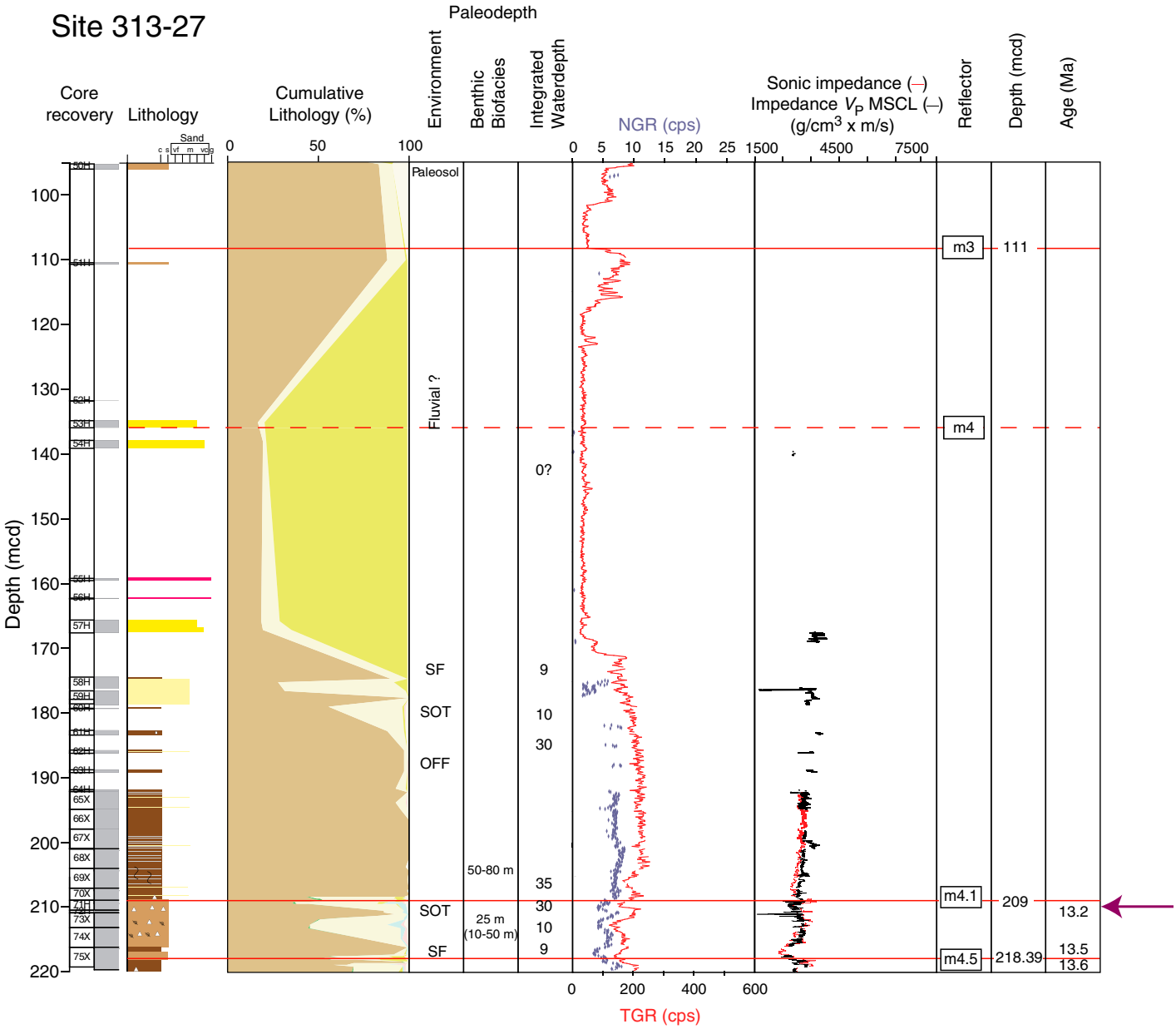

Figure 4. Integrated Ocean Drilling Program Expedition 313 Site M27 sequences m4.5–m3; depth is in meters composite depth (mcd). Explanation and key as in Figure 3. Ages for surface immediately below and above sequence boundaries are from Browning et al. (2013). Red—sonic impedance computed using downhole velocity and core density data; black—sonic impedance computed using core velocity and core density data. Dashed red lines—uncertain placement of sequence boundary. Purple arrow—placement of seismic sequence boundaries based on synthetic seismograms.

process resulted in the removal of values from a core data set, data were interpolated between values. No corrections were applied to account for differences between in situ formation velocities and those measured on the core; impedance values calculated from the sonic logs display higher values than those calculated from core velocities, although impedance contrasts occur at the same levels regardless of absolute values.

RESULTS

Eocene–Oligocene Sequence Boundaries

Eocene–Oligocene sequences were only sampled at Site M27 (Figs. 1 and 2). Sequence boundaries for the Eocene–Oligocene are identified based on hiatuses (Browning et al., 2013) associated with stratigraphic surfaces in the cores (Fig. 8) because the sequence boundaries have no resolvable seismic expression on Line 529 (Fig. 2). Pre-Miocene seismic resolution in the region of Expedition 313 degrades relative to the Miocene due to either increasing burial depth or less stratal organization, and the lack of visible reflector terminations hinders clear recognition of seismic sequence boundaries. Two poorly resolved Oligocene reflectors have been

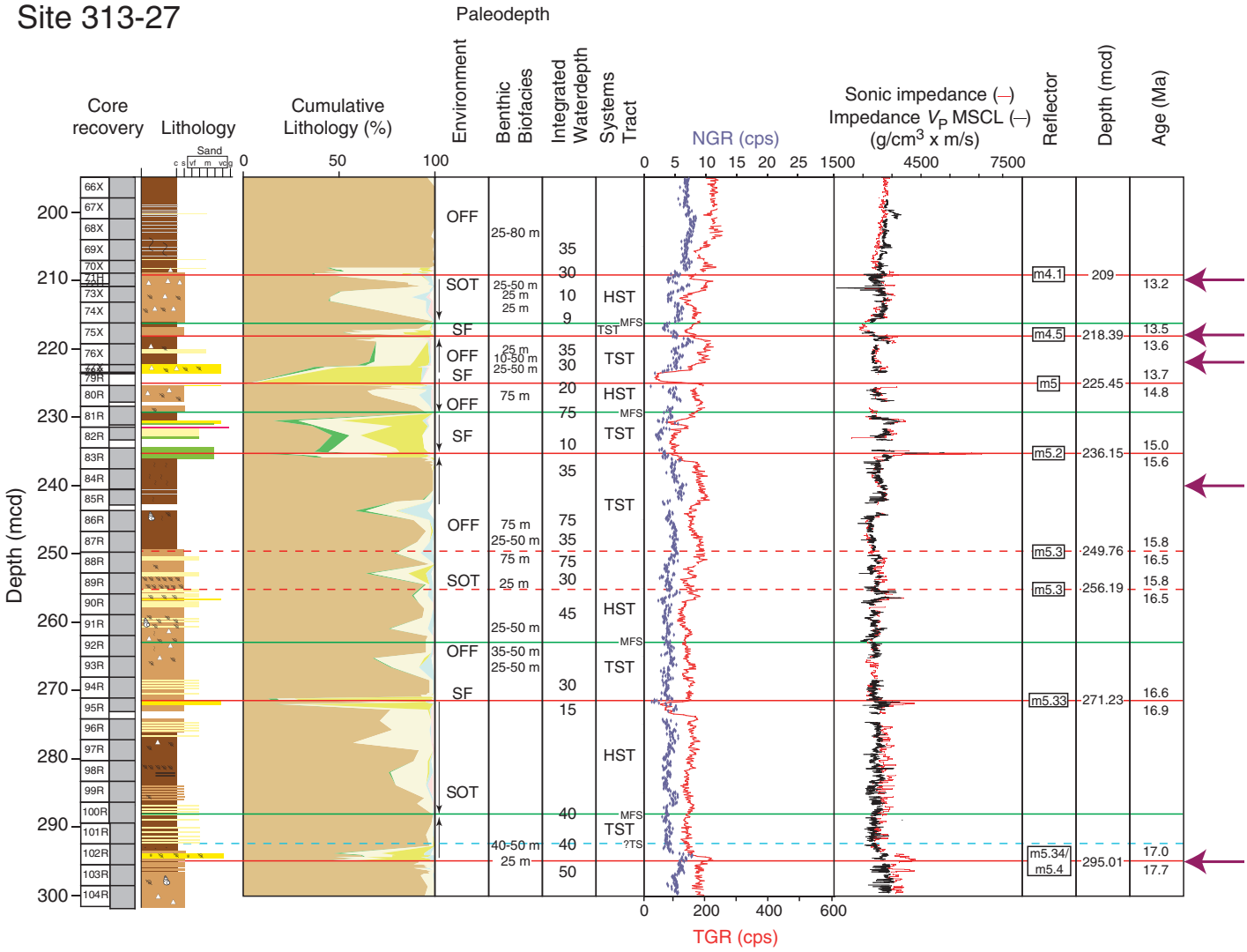

Figure 5. Integrated Ocean Drilling Program Expedition 313 Site M27, sequences m5.4–m4.1; depth is in meters composite depth (mcd). Explanation and key as in Figure 3. Green horizontal lines—maximum flooding surface (MFS); blue horizontal line—TS (transgressive surface; dashed where uncertain); systems tracts are discussed in text: LST—lowstand systems tract; TST—transgressive systems tract; HST—highstand systems tract. Purple arrows—placement of seismic sequence boundaries based on synthetic seismograms.

traced into Site M27, o.1 and o.5 (Fig. 2), both of which correlate within sequence O3 (Fig. 8). Eocene–Oligocene sequences at Site M27 were deposited on bottomsets (Fig. 2) in relatively deep water (generally 75–100 m paleodepth; Katz et al., 2013; Fig. 8) and their lithologic and seismic expressions are subtle. We identify one Eocene and three Oligocene sequences at Site M27.

Sequence O1

A distinct erosional surface at 625.83 m composite depth (mcd) (313–27–223R-1, 92 cm; Fig. 8; Fig. S1 in the Supplemental File [see footnote 1]) separates Zone NP21 below from Zone NP22 (Mountain et al., 2010; Browning et al., 2013) above and is interpreted as sequence boundary straddling the Eocene–Oligocene boundary. This irregular surface (spanning 5 cm) separates a glauconitic clay below from silty sand above (Fig. S1). The underlying Eocene sequence is poorly sampled. The overlying sequence O1 (625.83–617 mcd) is a glauconitic clay dated as ca. 32.3–32.2 Ma and correlated with onshore sequence O1 (Fig. 8) of Pekar et al. (2001); there appears to be a >1 m.y. hiatus (33.9–32.3 Ma) associated with the basal O1 sequence boundary, although this age assignment is tentative. Benthic foraminifera indicate deposition in 100–120 m paleodepth.

Sequence O3

A contact at 617 mcd (313–27–219R-1, 124 cm; Fig. 8; Fig. S2 in the Supplemental File [see footnote 1]) consists of an irregular (313–27–219R-1, 120–124 cm) burrowed surface (Fig. S2) with slightly shelly sandy silt above and sandy silt below; it is interpreted as a sequence boundary and is associated with a 2.9 m.y. hiatus from 32.2 to 29.3 Ma. This middle Oligocene sequence (617–538.68 mcd) is dated as 29.3–28.2 Ma (Fig. 8), correlating with onshore New Jersey sequence O3 of Pekar et al. (2001). Sequence O3 has three distinct sedimentary facies: a basal glauconitic-quartzose sandy clay (617–596.3 mcd), a medial glauconite

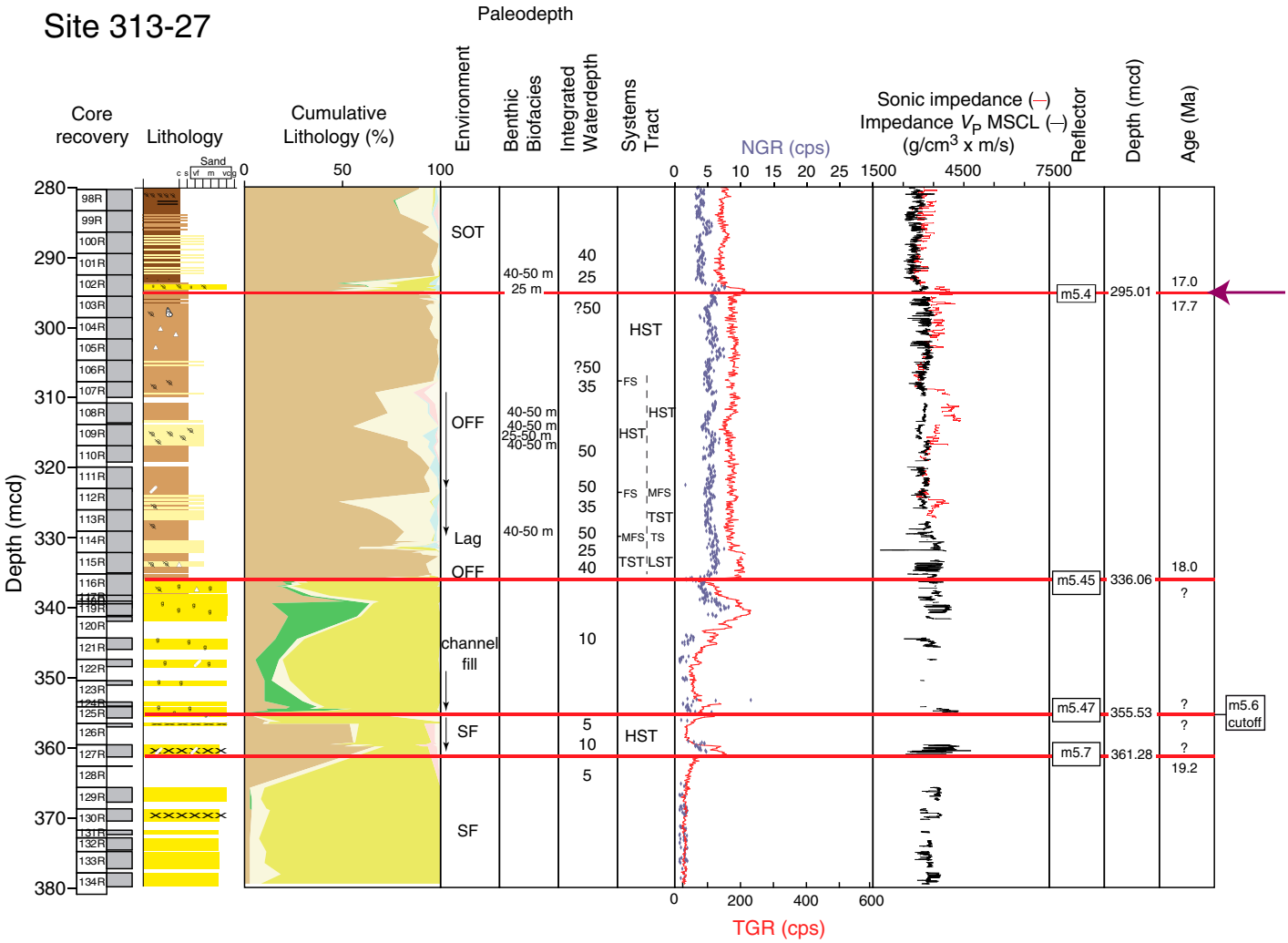

Figure 6. Integrated Ocean Drilling Program Expedition 313 Site M27, sequences m5.7–m5.4. Explanation as in Figures 3–5 (FS—flooding surface).

clay to clayey glauconite sand (596.3 to ~560 mcd), and an upper clayey glauconitic quartz sand (~560–538.68 mcd), all deposited in ~75–100 m of water. Reflector o.5 ties approximately to 563 mcd within sequence O3 at a glauconite peak (Fig. 8); synthetic seismograms confirm the depth placement of this reflector (level indicated with purple arrow, Fig. 8). A very poorly resolved reflector (o.1) is tentatively placed at 596.3 mcd using the revised velocity-depth function, a level of a large impedance contrast (Fig. 8); however, synthetic seismograms place it deeper (606 or 610 mcd; purple arrow, Fig. 8; Mountain and Monteverde, 2012). Considering the uncertainty in the depth of this reflector, it could be equivalent to the 617 mcd basal sequence boundary of sequence O3. Reflector o.1 may alternatively be associated with the facies change at 596.3 mcd because it is correlated with a major gamma-log increase and peak in mud, just below the facies change from clay to glauconite sands (Fig. 8). The sequence was deposited in relatively deep water (~75–100 m) influenced by entrainment and downslope transport indicated by the mixing of shallow-water and deep-water benthic foraminifera. Identification of an MFS is difficult on bottomsets and could be placed at either of the facies changes (596.3 or 563 mcd). A peak in *Uvigerina* spp. (typically found at MFS; Loutit et al., 1988) at 595.14 mcd (see Katz et al., 2013) favors the placement of the MFS at 596.3 mcd.

Sequence O6

A major hiatus (28.2–23.5 Ma) is associated with a heavily bioturbated contact at 538.68 mcd (313–27–191R-2, 70 cm; Fig. 8; Fig. S3 in the Supplemental File [see footnote 1]) separating glauconitic, slightly shelly fine sand below from silty fine sand above. The uppermost Oligocene sequence from 538.68 to 509/515 mcd is 23.5–23.0 Ma and apparently correlates with onshore sequence O6 (Pekar et al., 2001). It is dominated by clayey, slightly glauconite fine quartz sand (Fig. 8). Benthic foraminifera indicate ~75–100 m water depth.

Early to Middle Miocene Sequence Boundaries

Early to middle Miocene sequences show a distinct clinothem geometry beneath the New Jersey shallow shelf, with topsets, foresets, and bottomsets (Fig. 2). Water depths on the bottomsets are middle to outer neritic (typically 75–120 m; Katz et al., 2013), but due to complicated downslope transported sedimentary facies, correlation of

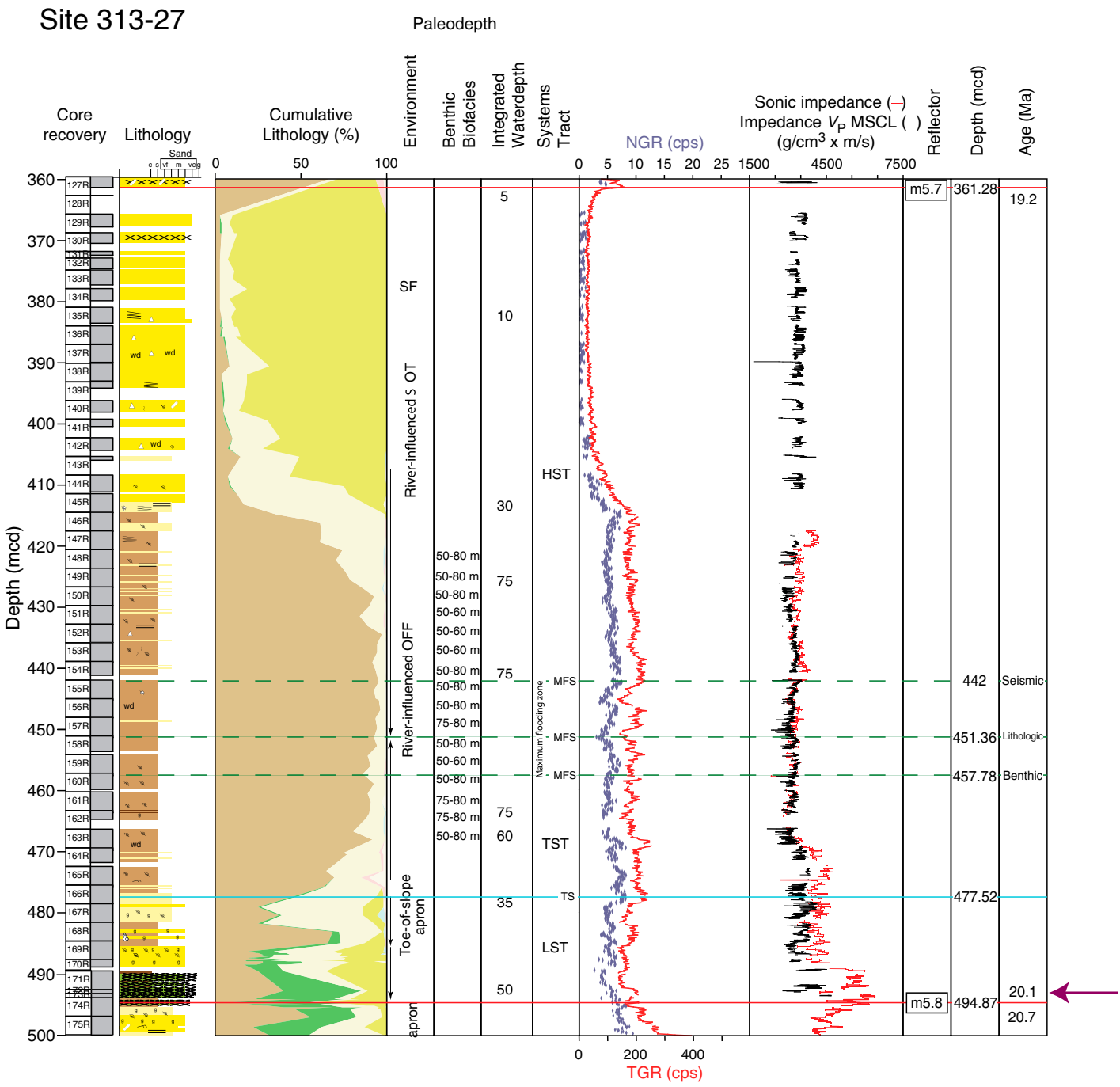

Figure 7. Integrated Ocean Drilling Program Expedition 313 Site M27, sequences m5.8–m5.7. Explanation and key as in Figures 3–5.

the seismic sequences to the core expressions of the sequence boundary is less clear on the bottomset than in proximal settings. Landward of the bottomsets, three sequences were drilled on the clinothem foresets: m5.8 at Site M27, m5.4 at Site M28, and m5.2 at Site M29, where placement of the sequence boundaries is clear (Fig. 2; see Miller et al., 2013b, for detailed discussion of these foresets). Placing seismic sequence boundaries on the topsets is potentially more complicated because these units are thin, although synthetic seismograms provide increased confidence in our correlations using the velocity-depth function (Mountain and Monteverde, 2012).

Sequence m6

Seismic sequence boundary m6 is placed at 509–515 mcd at Site M27 (Fig. 8). A coring gap (509–515 mcd) precludes definitively tying seismic sequence boundary m6, placed at 510 mcd by synthetic seismograms (Fig. 8), to impedance contrasts, although there is a major downhole increase in impedance just above the gap (Fig. 8). The impedance contrast is associated with an upsection increase in glauconite and large gamma-log increase (Fig. 8). At Site M27, the sequence consists of clayey glauconite-quartz sands deposited in a bottomset. Benthic foraminifera indicate a shallowing from ~75–100 m water depth at the base

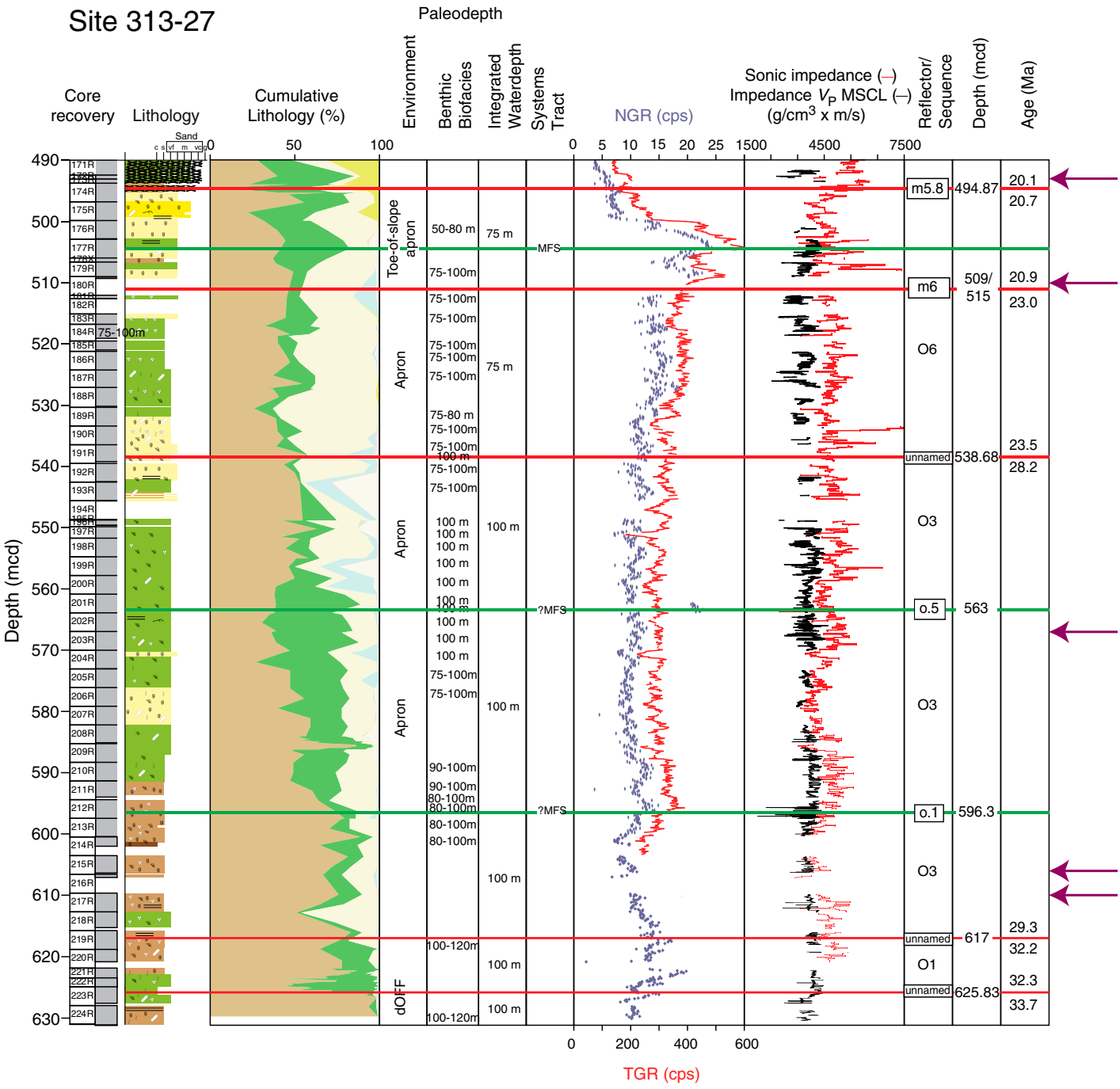

Figure 8. Integrated Ocean Drilling Program Expedition 313 Site M27, sequences from total depth to m5.8. Explanation and key as in Figures 3–5.

of the sequence to 50–80 m in the upper part of the sequence. This suggests that the glauconite bed at ~505 mcd may be an MFS (Fig. 8). Sequence m6 (509–494.87 mcd) is dated as 20.9–20.7 Ma at Site M27. The basal sequence boundary is associated with a long hiatus from 23.0 to 20.9 Ma, representing much of the Aquitanian, suggesting that reflector m6 truncates Aquitanian sequences. Onshore, the main Aquitanian sequence is Kw0, which reaches its maximum thickness at Cape May (Miller et al., 1997a; Browning et al., 2006); equivalent age strata are lacking in the Expedition 313 area. The m6 seismic sequence boundary was not cored at Sites M28 and M29 because it was below total depth.

Sequence m5.8

At Site M27, we cored the foreset of sequence m5.8 (Fig. 7). We note a distinct surface at 494.87 mcd (313–27–174R-1, 111 cm; Fig. 7; Fig. S4 in the Supplemental File [see footnote 1]) that separates graded, interbedded glauconite sand and clay below from quartzose glauconite sandstone above. This is the level

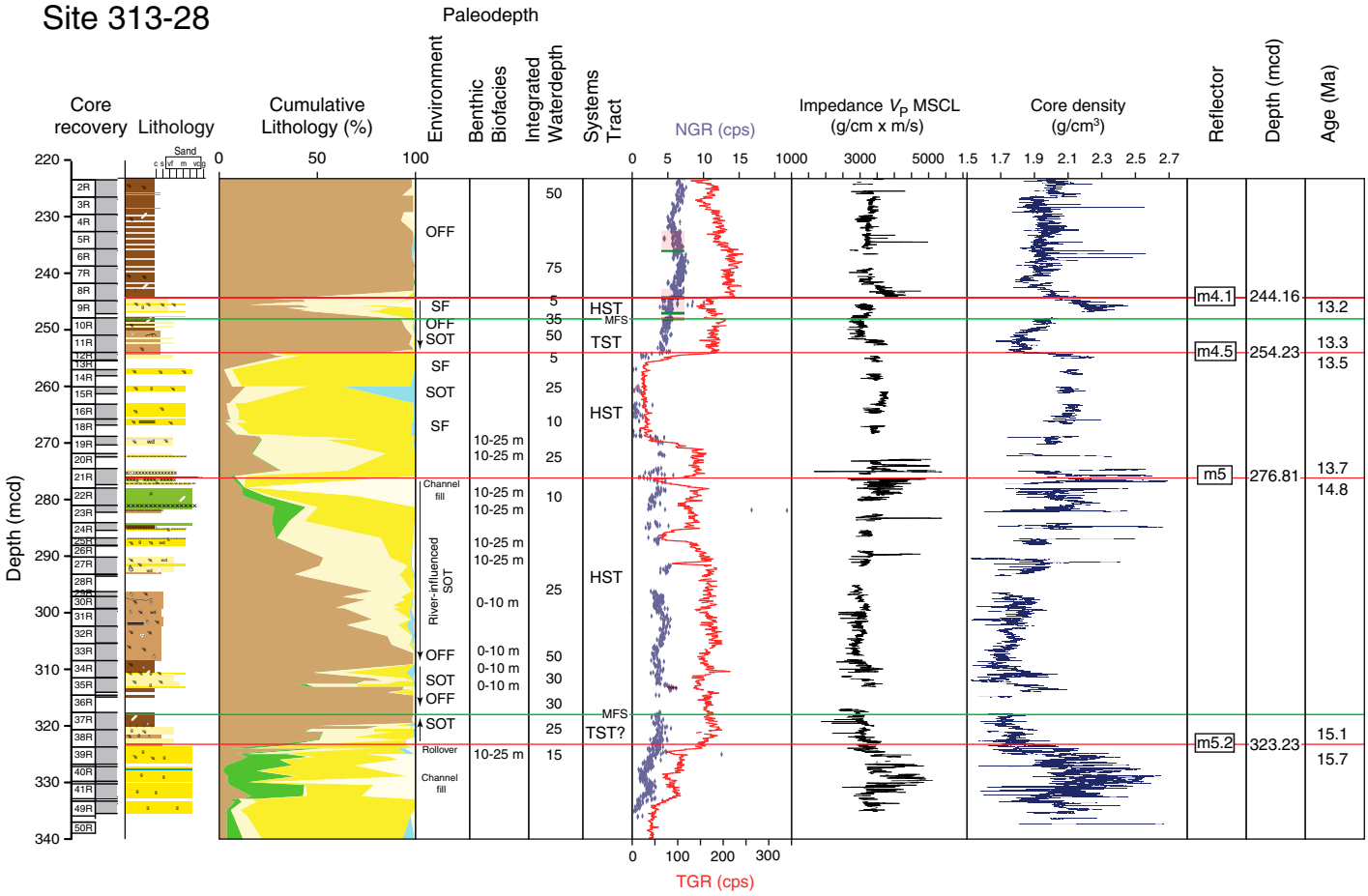

Figure 9. Integrated Ocean Drilling Program Expedition 313 Site M28, sequences 5.2–4.1. Explanation and key as in Figures 3–5.

predicted by the velocity-depth function for the seismic sequence boundary. Mountain et al. (2010) placed the sequence boundary at the top of the indurated zone (489.39 mcd). The top of the indurated zone is a major downhole increase in sonic impedance; the base and favored placement of the sequence boundary (Fig. 8) is a major decrease. Synthetic seismograms (purple arrow, Fig. 7) suggest that the m5.8 seismic sequence boundary is best placed at the lower contact (494.87 mcd). There are two coarsening-upward successions in the lower part of the sequence (494.87–485 mcd; 485–477.52 mcd) deposited on a bottomset. Benthic foraminifera are absent from samples in much of this lower section (494.77–469.895 mcd). We interpret this as a LST to 477.52 mcd and place the TS at the change from regressive to transgressive sedimentary facies at 477.52 mcd. This is overlain by a fining-upward succession to 451.36 mcd interpreted as a TST (see Miller et al., 2013b, for detailed discussion of systems tracts and stratal surfaces within this sequences). There is a large downhole increase in impedance at ~470 mcd and a decrease in impedance at 476 mcd; together, these two surfaces yield a strong positive (black) and negative (white) reflection just above the TS (Fig. 2). Placement of the MFS is uncertain, with three possible locations based on foraminiferal, lithologic, or seismic criteria: (1) at the top of the fining-upward TST at 451.36 mcd, where there is a shell concentration; (2) at 457.78 mcd, where peak abundance of planktonic foraminiferal at benthic foraminifera indicating maximum water depths within a thick zone of maximum water depth 50–80 m from 467.01 to 421.31 mcd; and (3) at 442 mcd, where we tentatively correlate a major downlap surface observed on seismic profiles (for further discussion see Miller et al., 2013b). The HST consists of offshore clays that continue to ~414 mcd, where there is an upsection coarsening to fine sands deposited in shoreface-offshore transition environments and overlain by medium- to coarse-grained sands deposited in shoreface environments. The m5.8 sequence is dated as 20.1–19.2 Ma at Site M27, with a 0.6 m.y. hiatus (20.7–20.1 Ma) associated with its basal unconformity. Considering that the m5.8 sequence at M27 captures a relatively complete cycle, this suggests that the hiatus is due to erosion and truncation of the underlying m6 sequence, as indicated on seismic profiles (Fig. 2).

At Site M28, there is a major contact at 662.98 mcd (313–28–169R-1, 61 cm; Fig. 12; Fig. S5 in the Supplemental File [see footnote 1]) that we correlate with seismic sequence boundary m5.8. The sequence boundary consists of glauconite sand over siltstone with large burrows extending to 27 cm below the contact (Fig. S5). Above this, sequence m5.8 (662.98–611.6 mcd) consists of tan prodelta silty clays; there were no benthic foraminifera in samples from this sequence. This placement of the sequence boundary is different from the depth predicted by the velocity-depth function (673 mcd, which is below the total depth of the hole) and no synthetic seismograms are available. However, we note a major downhole decrease in core density at 662.98 mcd (Fig. 12), and suggest that this is the best correlation considering that at both Sites M28 and M29, sequence m5.8 is associ-

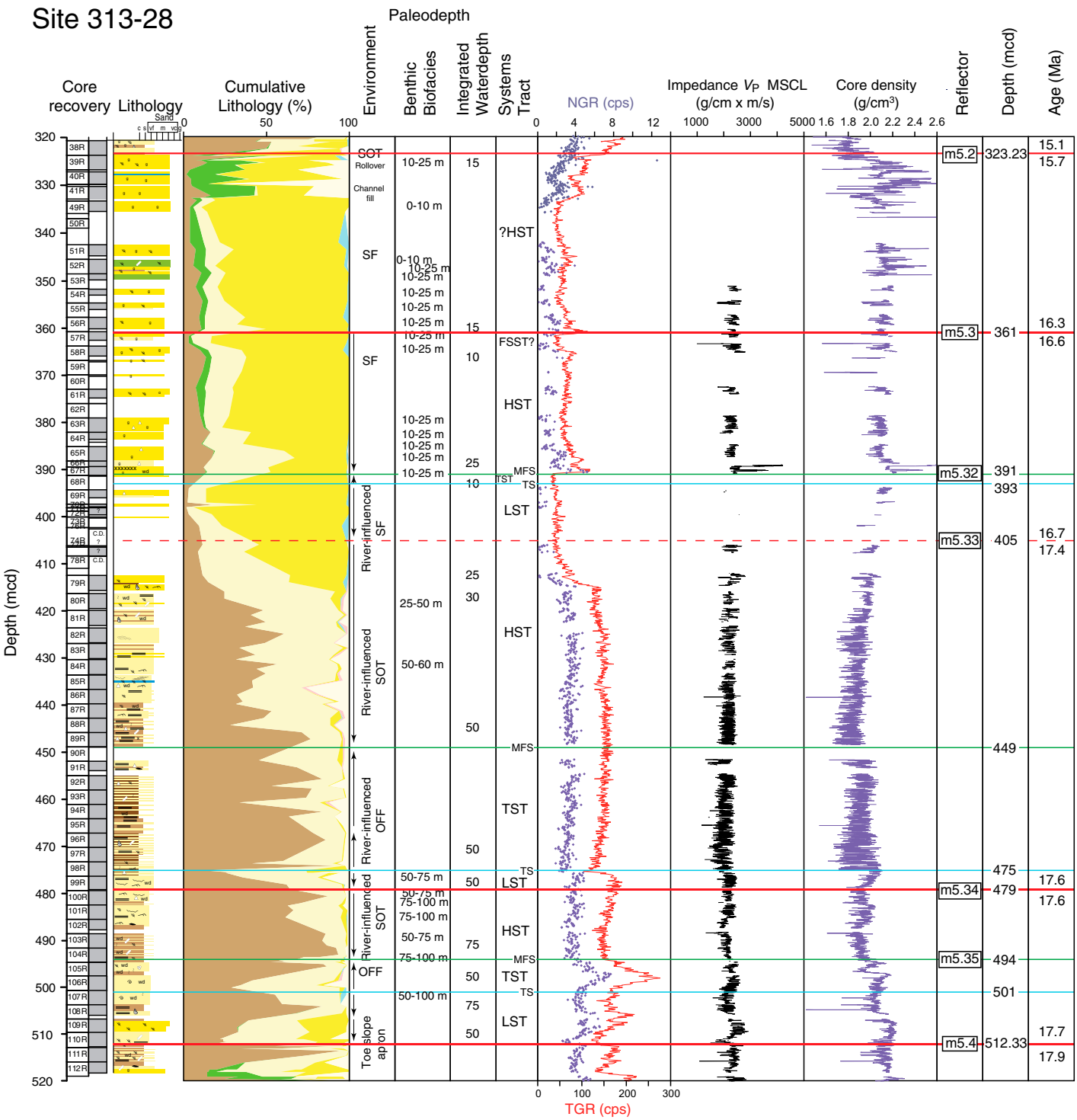

Figure 10. Integrated Ocean Drilling Program Expedition 313 Site M28, sequences 5.4–5.2. Explanation and key as in Figures 3–5.

ated with distinctive tan prodelta silty clays. Based on biostratigraphy alone, this sequence is dated as 20.0–19.5 Ma (Browning et al., 2013).

At Site M29, the velocity-depth function suggests that seismic sequence boundary m5.8 correlates at 747 mcd (Fig. 17). There are three surfaces in the core between 746 and 753.80 mcd (from top down: glauconite over clay, clay over glauconite clay, and the top of glauconite sands associated with a gamma-log peak); we lack velocity and density logs to differentiate which best matches the reflector, although it is likely that the gamma-log increase at 753.80 mcd marks the sequence boundary. We note that the prodelta silty clays overlie these closely spaced surfaces and that these extend to the top sequence boundary at 728.56 mcd. Benthic foraminifera in several samples at the base of the sequence indicate paleodepths of 75–100 m, and benthic foraminifera in a single sample at the top of the sequence indi-

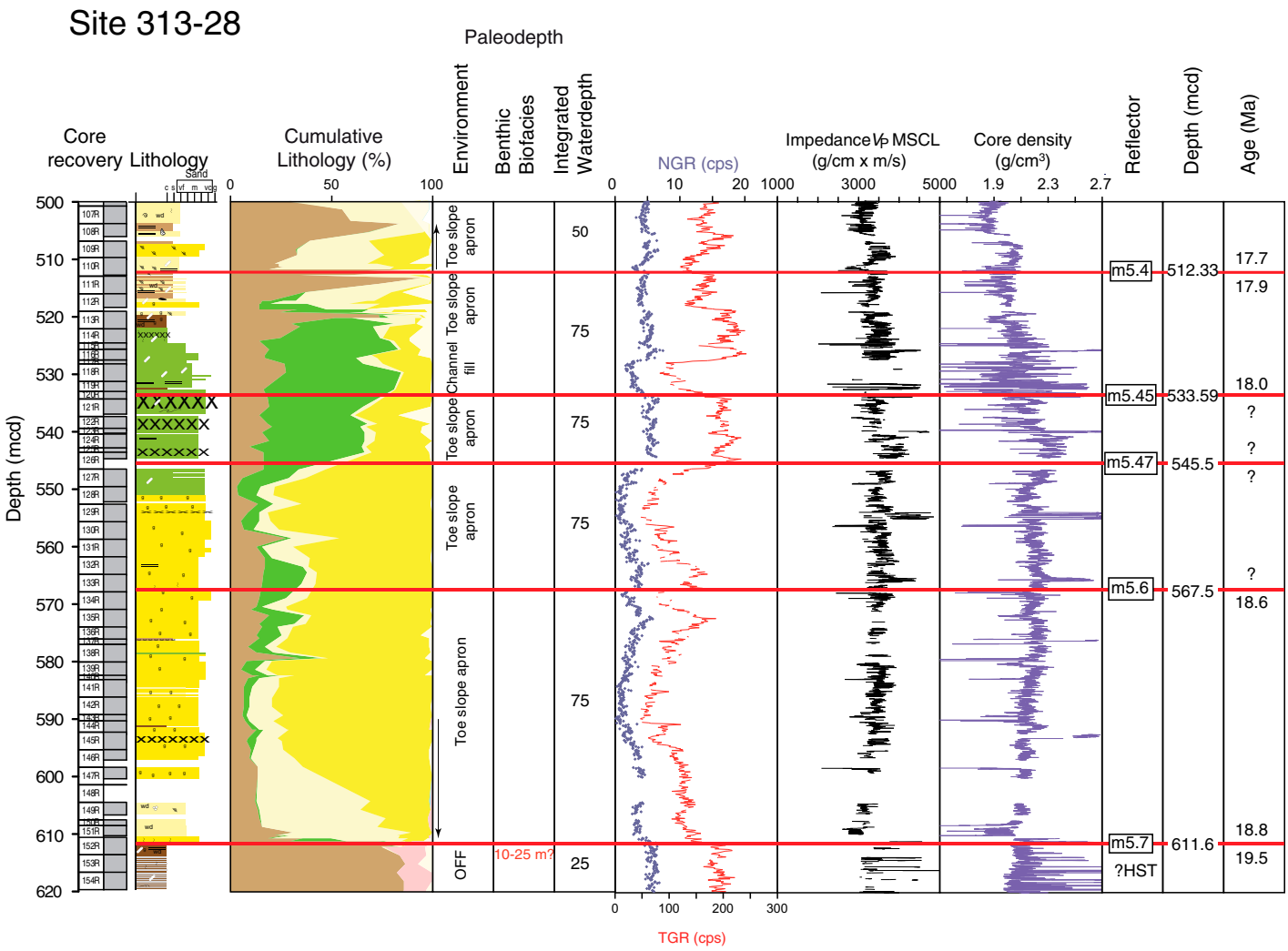

Figure 11. Integrated Ocean Drilling Program Expedition 313 Site M28, sequences m5.7–m5.4. Explanation and key as in Figures 3–5.

cate 50–80 m paleodepths; intervening samples are barren. We tentatively place the MFS at 742 mcd, at a change from sandy silt below to silty clay at a level where a downlap surface correlates to the corehole (Miller et al., 2013b). A seismic reflector links the HST sands of m5.8 at Site M27 with the prodelta clays at Sites M28 and M29. This sequence is poorly dated at Site M29 as 20.2–20.0 Ma (Browning et al., 2013).

Sequence m5.7

This sequence is poorly represented on Line 529 (Fig. 2). At Site M27, the m5.7 sequence boundary is placed in association with a large gamma-ray peak (361.28 mcd) in a coring gap separating indurated silty shoreface sands above from medium to coarse shoreface sands below (Fig. 6). The seismic sequence boundary is predicted at 365 mcd, but log data are insufficient to document an impedance contrast or allow computing of a synthetic seismogram. Seismic profiles show this sequence as a thin remnant overlying the clinoform rollover of the underlying sequence. This thin (5.75 m) sequence coarsens upsection, likely reflecting an HST. Absence of foraminifera in this sequence is consistent with the interpretation of shallow-water shoreface deposits. The sequence boundary cannot be dated at this site.

At Site M28, the basal m5.7 sequence boundary is placed at a very heavily bioturbated sequence boundary at 611.60 mcd (313–28–152–R1, 108 cm; Fig. 11; Fig. S6 in the Supplemental File [see footnote 1]) separating a medium sand above from a clay below, associated with a major downhole gamma-log increase. Heavy bioturbation extends 30 cm above and below the contact. A major downhole increase in impedance is caused by a density increase from the sands to the clays (Fig. 11). The sequence coarsens upsection to ~595 mcd; above this, it consists of fairly uniform medium sands, devoid of foraminifera, deposited on a bottomset (Fig. 11). Distinct seismic downlap onto sequence boundary m5.7 at Site M28 suggests that this upward coarsening occurs in the HST. The m5.7 sequence is poorly dated at Site M28, with a best age estimate of 18.8–18.6 Ma and a hiatus of ~0.7 m.y. (19.5–18.8 Ma) at the basal sequence boundary.

At Site M29, the basal m5.7 sequence boundary is placed at a heavily burrowed contact at 728.56 mcd (313–29–208-R1, 9–11 cm; Fig. 17; Fig. S7 in the Supplemental File [see footnote 1]) separating glauconitic quartz sands above from tan prodelta clays below. Burrows extend more than 30 cm below the contact. This change is associated with an uphole gamma-log increase due to high abundance of glauconite. Sonic data are insufficient to demonstrate that this is an impedance contrast and no synthetic seismogram is available, although there is a major minimum in core density at the sequence boundary, suggesting a likely large impedance contrast (Fig.

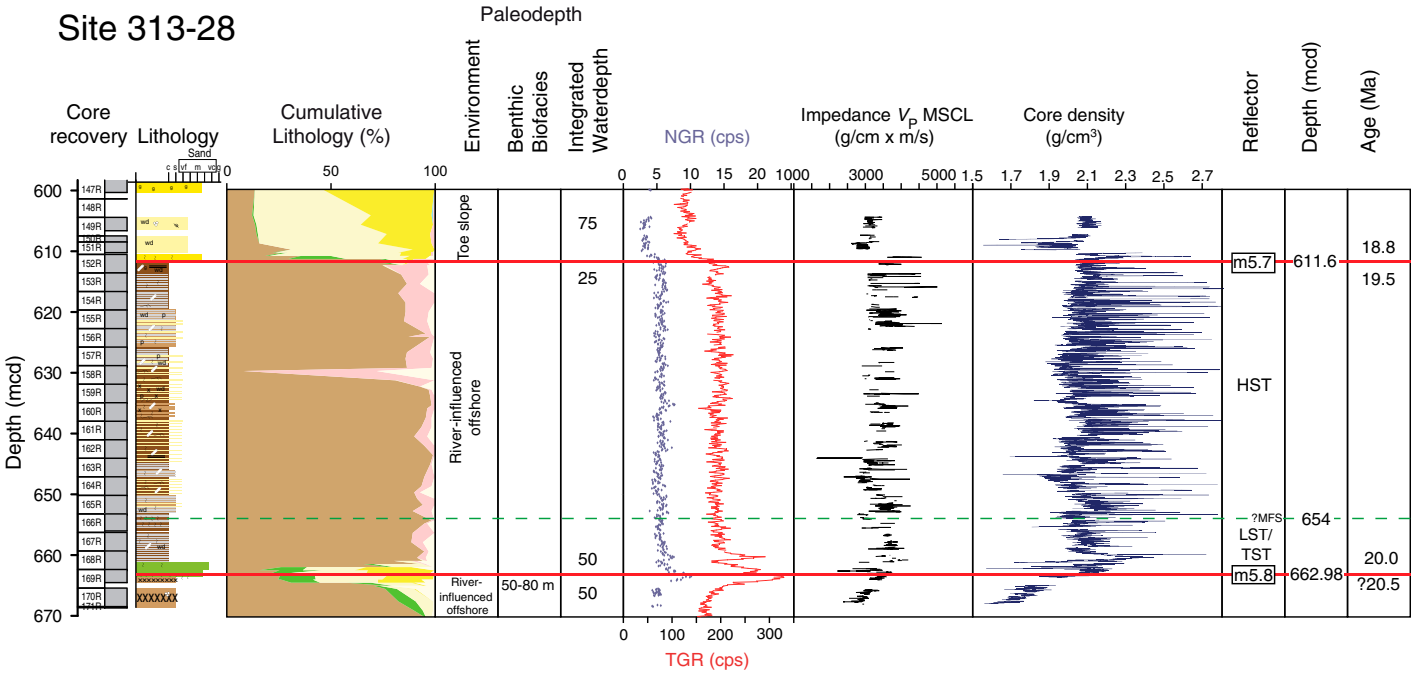

Figure 12. Integrated Ocean Drilling Program Expedition 313 Site M28, sequences from total depth to m5.7. Explanation and key as in Figures 3–5.

17). The sequence (728.56–707.56/710 mcd) fines upward from a bottomset sand to a clay. It was deposited on a bottomset in ~75 m water depth and is dated as ca. 18.8–18.6 Ma. Benthic foraminifera indicate paleodepths of 75–100 m in most of the sequence.

Sequence m5.6

This sequence is cut out at Site M27 (Fig. 2). At Site M28, the revised velocity depth function places this sequence boundary at 567.5 mcd associated with an uphole gamma log increase. No distinct unconformity was observed in the cores and medium-coarse sand occurs across the boundary, though there is a distinct increase in glauconite above the boundary (Fig. 11). Our placement of the sequence boundary at 567.5 mcd differs from that in Mountain et al. (2010), wherein the basal m5.6 sequence boundary was placed at 545.5 mcd; we now place the m5.47 sequence boundary at 545.5 mcd based on the revised velocity-depth function (Fig. 11). There is a large impedance contrast just above 567.5 mcd (Fig. 11). The sequence at Site M28 is a bottomset sand devoid of foraminifera and cannot be dated.

At Site M29, the m5.6 sequence boundary is placed in a coring gap (707.56–710 mcd) with glauconitic quartz sand above and silt below (Fig. 17). Despite the coring gap, log data suggest a major impedance contrast associated with the sequence boundary (Fig. 17), and synthetic seismograms place the reflector just below this level (>715 mcd; purple arrow, Fig. 17). The sequence (707.56/710–696/687.87 mcd) consists of a muddy glauconitic fine-coarse sand deposited in a bottomset, with glauconite increasing upsection (Fig. 17). Most of the sequence is barren of benthic foraminifera, except two samples at the top of the sequence that indicate paleodepths of 90–120 m. The m5.6 sequence at Site M29 is dated as 18.3–18.1 Ma with a 0.3 m.y. hiatus at its base (18.6–18.3 Ma). Sequence m5.5 is eroded in the Expedition 313 area and is not discussed here.

Sequence m5.47

Seismic profiles show that the m5.47 sequence is highly dissected by erosion between Sites M27 and M28; the clinoform rollover is heavily eroded on Line 529 (Fig. 2), although it is well imaged in nearby areas (Monteverde et al., 2008). This erosion cut out the m6 sequence at Site M27. We place the basal m5.47 sequence boundary at 355.53 mcd (313–27–125–1, 140 cm; Fig. 6; Fig. S8) at the top of a cemented quartz sandstone overlain by a glauconitic quartz sand associated with an upsection gamma-log increase. The sands (355.53–336.06 mcd) are interpreted as channel-fill deposits (Mountain et al., 2010) that are barren of foraminifera. The log quality in this section is not good due to gaps; no impedance data are available across the sequence boundary and no synthetic seismogram was computed. This sequence cannot be dated at this site or at Site M28.

At Site M28, we place the basal m5.47 sequence boundary at 545.5 mcd in a coring gap separating indurated glauconite sand above from glauconitic medium-coarse sand below associated with a major upsection gamma increase (Fig. 11). There is an increase in impedance upsection due to a density increase associated with the lithologic change (Fig. 11). The sequence consists of glauconite-quartz sands devoid of foraminifera deposited on a bottomset (Fig. 11); it cannot be dated at this site.

The placement of the basal m5.47 sequence boundary at Site M29 is uncertain, and it can be placed at either 687.87 mcd at the top of a silt (Mountain et al., 2010) and a downhole decrease in impedance, or at ~696 mcd at the contact of the silt with underlying granuliferous glauconite-quartz sands and a downhole increase in density (no sonic velocity data are available in this interval to compute impedance; Fig. 17; Fig. S9 in the Supplemental File [see footnote 1]). There is a heavily bioturbated contact at 695.65 mcd (313–29–196R-1R, 74 cm; Fig. S9) that is the likely placement of the sequence boundary. The sand and clay couplets mark deposits on the bottomset, with sands generally at the base and clays at top (e.g., sequence m5.7; Fig. 17), which would favor the upper placement (687.87 mcd). However, synthetic seismograms suggest placement at the lower contact (695.65 mcd), as does the heavily bioturbated surface (Fig. S9). The sequence is dated as ca. 18.0–17.9 Ma.

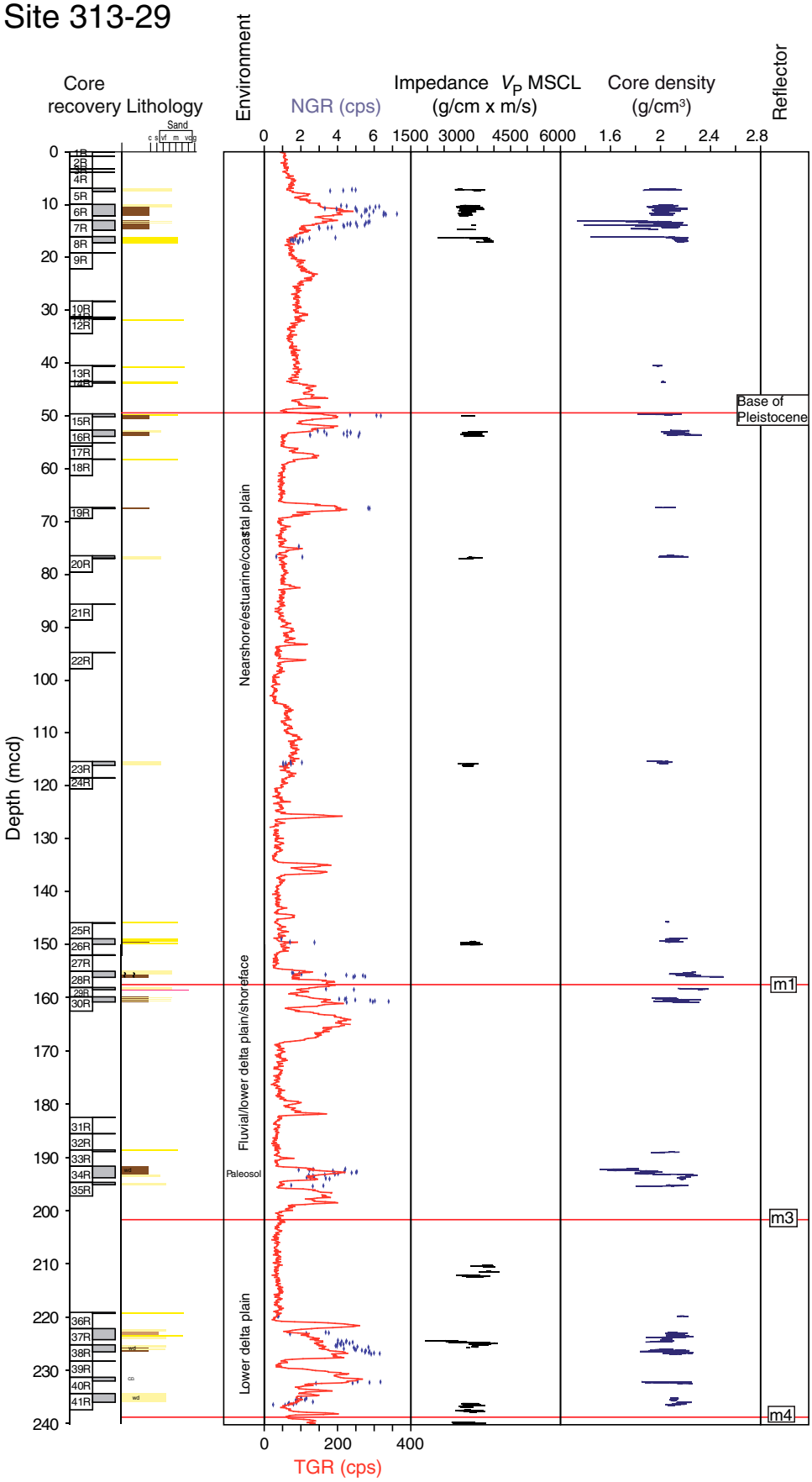

Figure 13. Integrated Ocean Drilling Program Expedition 313 Site M29, sequence m4 and younger sequences. Explanation and key as in Figures 3–5.

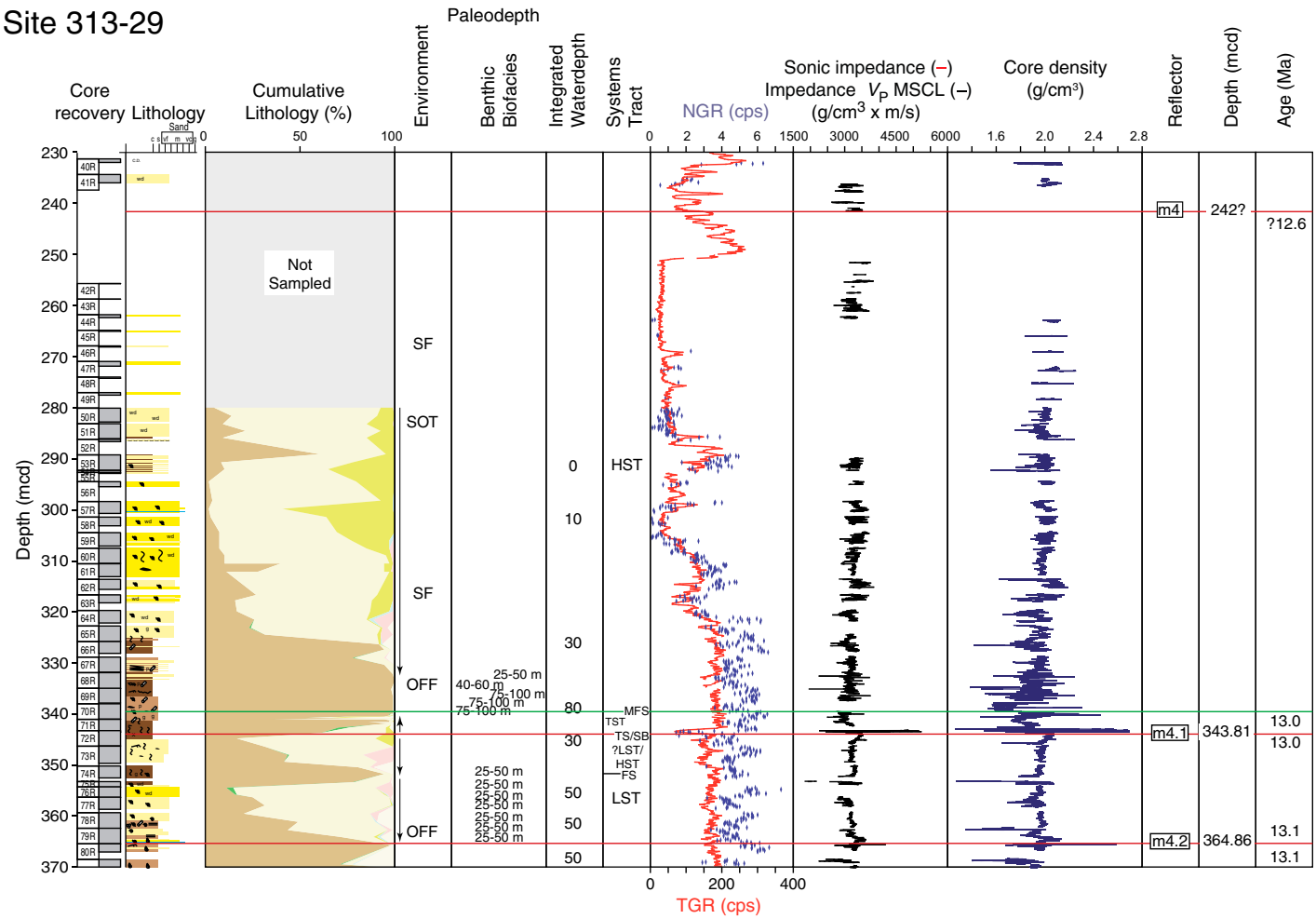

Figure 14. Integrated Ocean Drilling Program Expedition 313 Site M29, sequences m4.1–m4. Explanation and key as in Figures 3–5.

Sequence m5.45

Seismic profiles (Fig. 2) show that the m5.45 sequence erodes into m5.47. The topsets and bottomsets of m5.45 were eroded by the overlying m5.4 sequence boundary, but the foreset of the m5.45 clinoform is imaged between Sites M27 and M28 (Fig. 2). Expedition 313 sampled sequence m5.45 in a truncated topset at Site M27 and eroded bottomsets at Sites M28 and M29. At Site M27, the basal sequence boundary of m5.45 is placed at 336.06 mcd (313–27–116–1, 90 cm; Fig. 6; Fig. S10 in the Supplemental File [see footnote 1]) at an erosional contact of a silt over a slightly glauconitic coarse quartz sand associated with an upsection gamma-log increase. No impedance contrast appears to be associated with this contact, although log quality in this section is not good due to spotty sampling and no synthetic seismogram is available. The lithology within the sequence shows two distinct coarsening-upward parasequences (329–323 and 323–309 mcd) within an otherwise fine-grained unit. Based on their location on the topset, we interpret this sequence as dominantly HST (Fig. 6). Benthic foraminifera indicate paleowater depths of ~25–50 m (probably 40–50 m) for 329.81 mcd and 311.46–318.81 mcd. Abundant planktonic foraminifera (~7%–41%) also characterize these sections; however, most samples below and above these intervals are barren except for 295.01 mcd (~25 m). We tentatively place the MFS at a mud peak at 329.81 mcd and interpret flooding surfaces at ~323 and 308 mcd within the HST. This is consistent with apparent placement of a downlap surface at ~330 mcd, although correlation into the corehole is not certain. An alternative interpretation (Fig. 6) places the downlap surface and MFS at ~323 mcd at the highest mud peaks, interprets the lag at ~332 mcd as the TS, and places a thin LST below this. Sequence m5.45 is dated as 18.0–17.7 Ma at Site M27; the basal hiatus cannot be dated, although it is <1.2 m.y.

At Site M28, the basal sequence boundary of m5.45 is placed at the top an indurated zone at 533.59 mcd (313–28–120R-1, 63 cm; Fig. 11; Fig. S11 in the Supplemental File [see footnote 1]) with angular glauconite sands above (channel fill of Mountain et al., 2010) and glauconite sandstone below associated with a major gamma-log decrease upsection. A large downhole density drop causes a large impedance contrast at this surface (Fig. 11). Glauconite decreases and quartz increases in the upper part of the sequence (~520–512.33 mcd; Fig. 11). The sequence was deposited on a bottomset (Fig. 2). No benthic foraminifera were found in this sequence at Site M28. The m5.45 sequence is dated as 18.0–17.9 Ma at Site M28; the hiatus associated with the basal sequence boundary cannot be dated, although it is <0.6 m.y.

The placement of the basal m5.45 sequence boundary at Site M29 is uncertain, and it can be placed at either 673.71 mcd at the contact of a glauconite sand over a silty clay (313–29–189R-1, 15 cm; Mountain et al., 2010; Fig. S12 in the Supplemental File [see footnote 1]) and a downhole decrease in impedance, or at 683.17 mcd at the contact of the silty clay with underly-

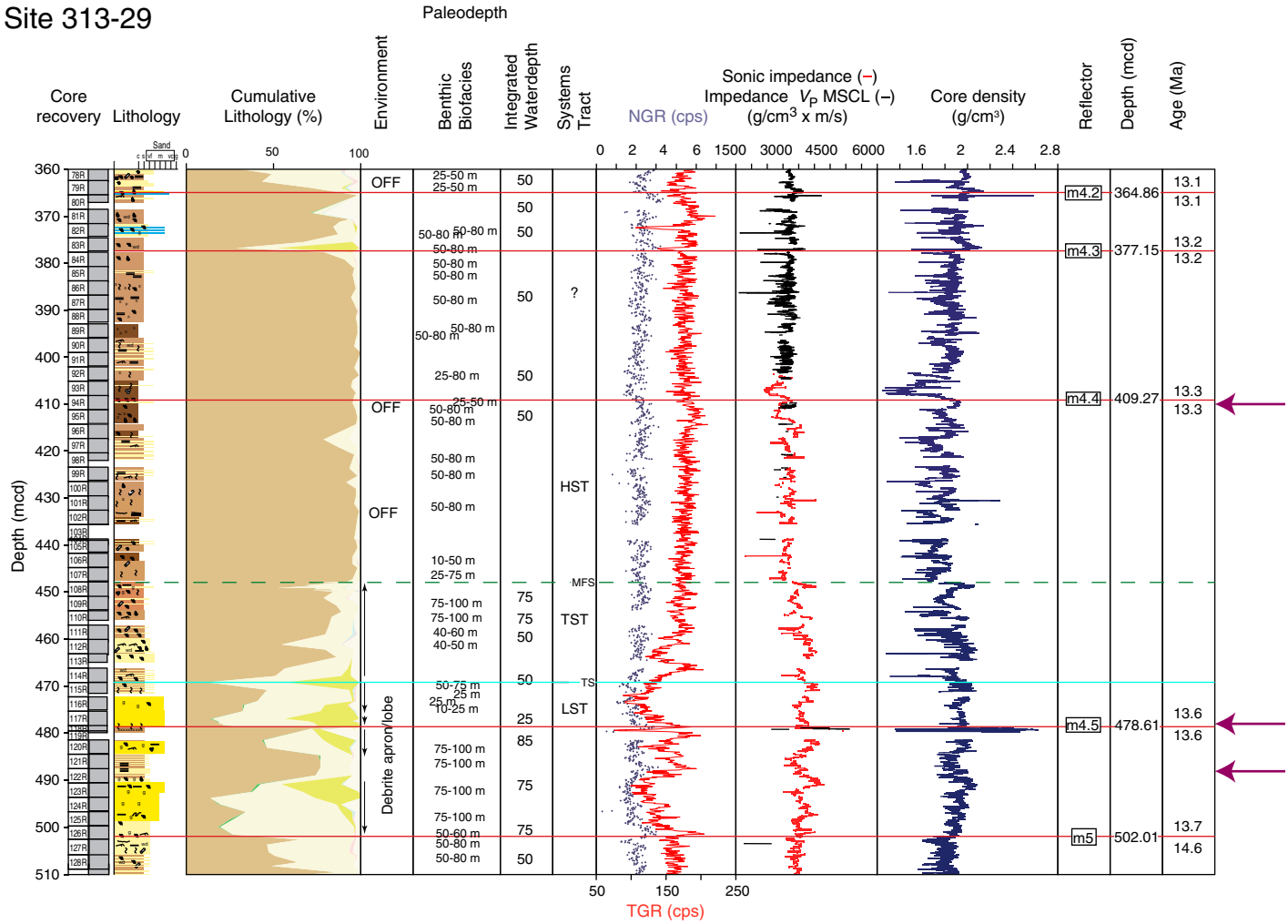

Figure 15. Integrated Ocean Drilling Program Expedition 313 Site M29, sequences m5–m4.2. Explanation and key as in Figures 3–5.

ing glauconite-quartz sands (313–29–192R-1, 46 cm) and a downhole increase in impedance (Fig. 17; Fig. S13 in the Supplemental File [see footnote 1]); synthetic seismograms (purple arrow, Fig. 17) favor the latter, placing it at 683.17 mcd. The sequence is dated as 17.8 or 17.9–17.7 Ma.

Composite Sequence m5.4

A major conclusion in Miller et al. (2013b) is that m5.4 is a composite sequence that may be divided into three higher order (100–400 k.y. scale) sequences separated by reflectors m5.34 (479 mcd) and m5.33 (405 mcd) based on detailed evaluation of seismic, core, and stacking patterns. Details of systems tracts are presented in Miller et al. (2013b); we focus here on the impedance contrasts associated with these sequence boundaries.

Site M28 cored sequence m5.4 in a foreset, with several intrasequence reflections (m5.35, 5.34, 5.33, 5.32; Figs. 2 and 10 herein, in addition to several other numbered surfaces in Miller et al., 2013b). The basal m5.4 sequence boundary is placed at 512.33 mcd (313–28–110R-2, 114 cm; Fig. 10; Fig. S14 in the Supplemental File [see footnote 1]) at a distinct contact of fine sand over clayey silt. This differs slightly from Mountain et al. (2010), wherein it was placed at a surface at 495.2 mcd, where there is a thin sand bed over a clayey silt. There is only a minor impedance contrast associated with the sequence boundary (synthetic seismogram data are not available), perhaps because toe-of-slope facies are juxtaposed across the contact with a minimal time gap (ca. 17.7 Ma above, 17.9 Ma below). This is surprising considering the high amplitude of reflector m5.4 (Fig. 2). The overall million-year-scale m5.4 sequence (512.33–361 mcd) could be interpreted as one thick (151 m) sequence and dated as 17.7–16.6 Ma. However, examination of seismic profiles shows that reflectors m5.34 and 5.33 are seismic sequence boundaries that subdivide this composite sequence (sensu Mitchum and Van Wagoner, 1991; Neal and Abreu, 2009). Chronostratigraphic constraints support that these are sequences on the 100–400 k.y. scale (Browning et al., 2013). Sequence boundary m5.34 (predicted at 479 mcd) is associated with a minor impedance contrast (Fig. 1), whereas sequence boundary m5.33 (405 mcd) is placed in a coring gap (400.30–412.47 mcd). The m5.34 sequence boundary may be lithologically expressed at the contact of very fine sand over silt at 313–28–100R-1, 77 cm (480.14 mcd). No synthetic seismograms are available for this site. (For details of the MFS, TS, and systems tracts and ages of these sequences, see Miller et al., 2013b.)

At Site M27, the basal sequence boundary of m5.4 is placed at an erosional surface at 295.01 mcd (313–27–102R-2, 105 cm; Fig. 5; Fig. S15 in the Supplemental File [see footnote 1]) based on the revised velocity-depth function

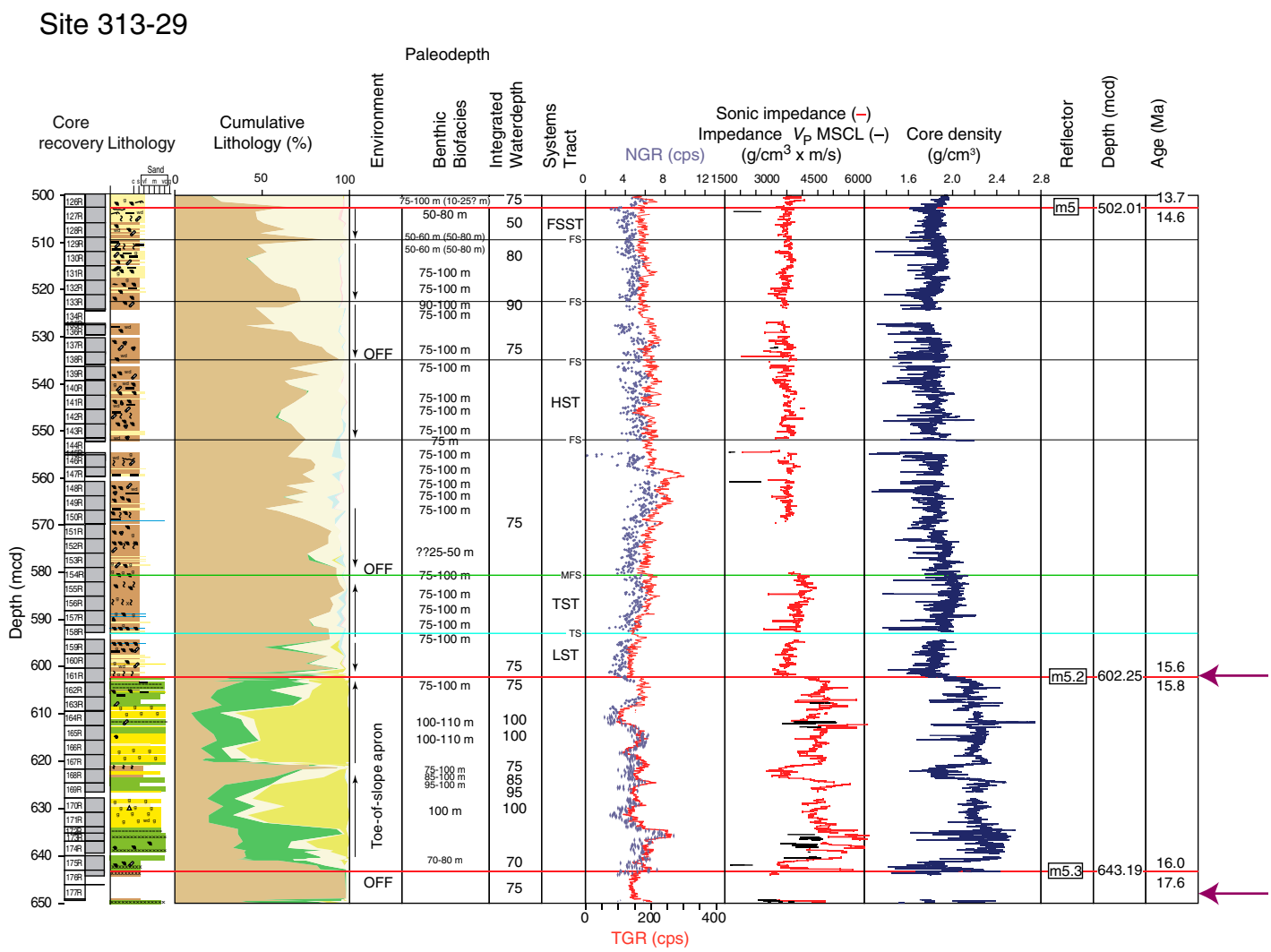

Figure 16. Integrated Ocean Drilling Program Expedition 313 Site M29, sequences m5.3–m5. Explanation and key as in Figures 3–5.

where a very coarse sand lag overlies a silt (Mountain et al., 2010). This contrasts with the previous placement at 271.23 mcd (Mountain et al., 2010), which is here identified as higher order sequence boundary m5.33 (Miller et al., 2013b). Both surfaces at 295.01 and 271.23 mcd yield impedance contrasts, although synthetic seismograms unequivocally link seismic sequence boundary m5.4 with the lower surface (purple arrow, Fig. 5). The m5.4 composite sequence at Site M27 appears to consist of the m5.34 and m5.33 higher order sequences. The m5.34 sequence (295.01–271.23 mcd) has a possible TS at 292 mcd and a possible MFS at ~289 mcd (Fig. 5). Facies trends above the 271.23 mcd m5.33 sequence boundary are unclear, although benthic foraminifera indicate maximum water depth at the correlation of a downlap surface at 263 mcd, suggesting placement of the MFS (Miller et al., 2013b), and shallowing upward in the HST from 263 to the overlying sequence boundary, although HST sands are absent. Placement of the upper sequence boundary (249.76/256.19 mcd) is unclear (see discussion of sequence m5.3). The m5.34 sequence at Site M27 is dated as 17.0–16.9 Ma, with a hiatus of 0.7 m.y. associated with the basal sequence boundary (17.7–17.0 Ma). The higher order sequence m5.33 (271.23–256.19 mcd; discussed in Miller et al., 2013b) is dated as 16.6–16.5 Ma (Fig. 5).

At Site M29, the m5.4 sequence boundary is placed at 662.37 mcd (313–29–183R-1, 101 cm; Fig. 17; Fig. S16 in the Supplemental File [see footnote 1]), where a silt overlies a silty glauconite sand associated with a very large downhole density and impedance increase. Synthetic seismograms place the m5.4 seismic sequence boundary at this level (purple arrow, Fig. 17). The sequence (662.37–643.19 mcd) consists primarily of silt with floating granules and coarse quartz sand (Mountain et al., 2010) deposited on a bottomset and dated as 17.7–17.6 Ma at this site with no discernible gap at its base. The entire sequence is characterized by outer middle neritic (75–100 m) foraminiferal assemblages.

Sequence m5.3

The placement of the basal sequence boundary of m5.3 is equivocal at Site M27 (Fig. 5). In Mountain et al. (2010), m5.3 was placed at 236.15 mcd, where we now place sequence boundary m5.2 (Fig 2). The revised velocity-depth function places m5.3 near 249.76 mcd at the level of a contact of clay above and sandy silty clay below. Alternatively, a bioturbated contact at 256.19 mcd (313–27–90–1, 33 cm; Fig. 5; Fig. S17 in the Supplemental File [see footnote 1]) separating coarse glauconite and granules above from silt below is another possi-

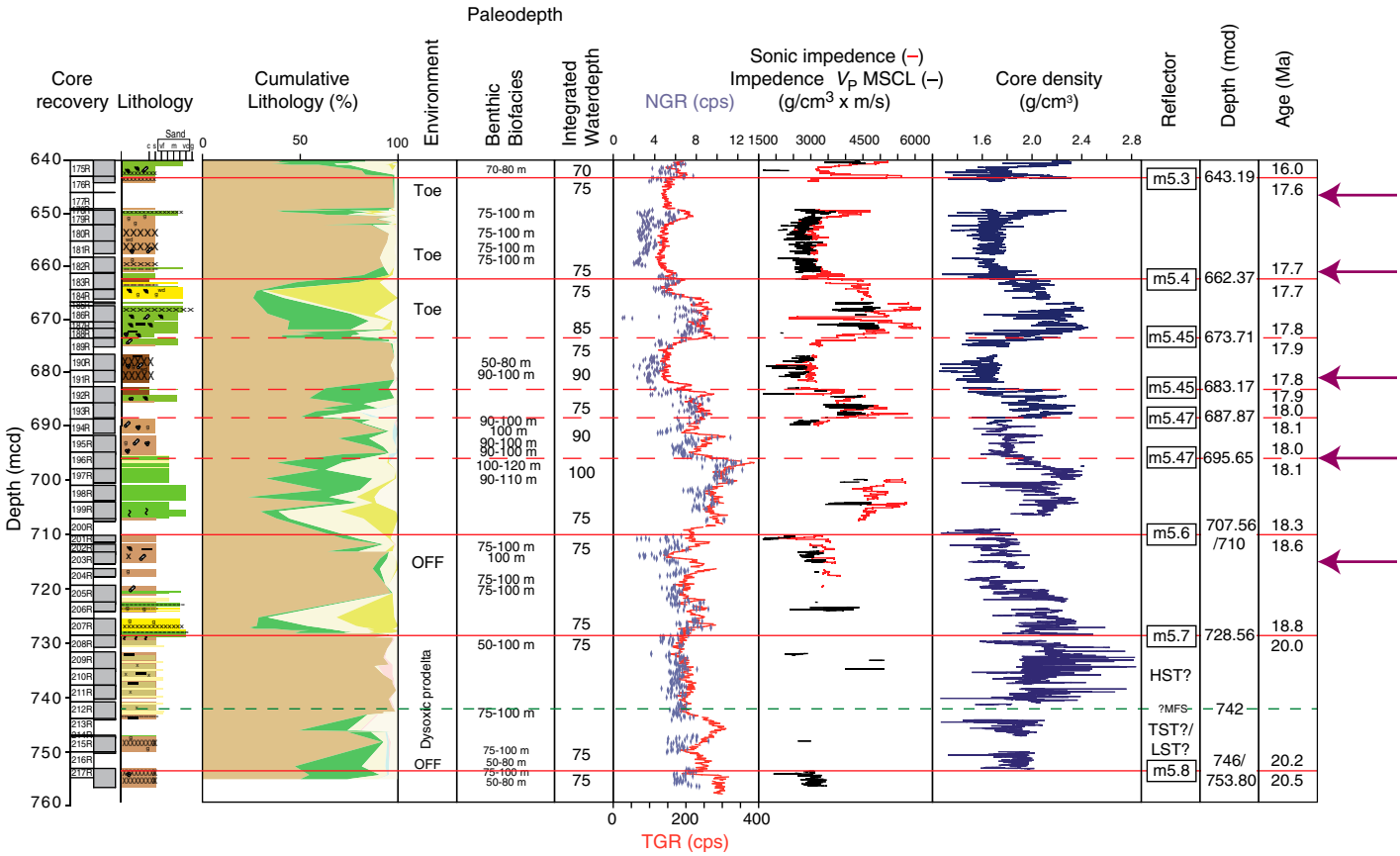

Figure 17. Integrated Ocean Drilling Program Expedition 313 Site M29, from total depth to sequence m5.3. Explanation and key as in Figures 3–5.

ble placement of the m5.3 sequence boundary at Site M27. This lower surface yields a relatively sharp impedance contrast (Fig. 5). This contrast did not yield a reflector on the synthetic seismogram because of destructive interference with the SMT-generated wavelet. We favor placement at 256.19 mcd based on the core expression (Fig. S17). The sequence (256.19–236.15 mcd) was drilled on a topset and appears to consist of one or two fining-upward successions (depending on choice of the placement of the sequence boundary) interpreted as a TST with an MFS near the top of the sequence. Foraminifera indicate an upsection deepening from ~25 m (255.06 mcd) to ~25–75 m (250.46–245.88 mcd), overlain by barren samples. It is dated as 15.8–15.6 Ma, with a hiatus of 0.7 m.y. associated with the basal sequence boundary (16.5–15.8 Ma).

At Site M28, the basal m5.3 sequence boundary is predicted at 361 mcd; we place it here at a major gamma-log change (Fig. 10). There is little expression of this sequence boundary in the core; it is likely in a small coring gap separating a coarse sand below 360.74 mcd and a fining-upward fine to medium to coarse sand from 360.13 to 359.0 mcd. This sequence was drilled on a topset immediately landward of the rollover of the underlying clinothem and consists of a thick pile of coarse slightly glauconitic quartz sands deposited in shoreface environments and capped by a channel (Mountain et al., 2010). This sequence is apparently regressive and is interpreted as an HST. Foraminiferal assemblages are consistent with this conclusion, with paleodepths of 10–25 m through 346.26 mcd, 0–10 m for 345.81–336.07 mcd, and barren above this, with the exception of 10–25 m at 324.42 mcd. The sequence is dated as 16.3–15.7 Ma, with a short hiatus (0.3 m.y.) associated with the basal sequence boundary (16.6–16.3 Ma).

At Site M29, the basal m5.3 sequence boundary is placed at 643.19 mcd (313–29–176R-1, 13 cm; Fig. 16; Fig. S18 in the Supplemental File [see footnote 1]) at an abrupt, irregular contact where overlying glauconite sand is burrowed down (67 cm) into silt and associated with a large impedance contrast. Synthetic seismograms place the m5.3 seismic sequence boundary in a coring gap just below this level (648 mcd); the discrepancy is likely due to interpolation of data by SMT across the data gap. The sequence (643.19–602.25 mcd) was deposited on a bottomset with two distinct coarsening-upward successions separated by a silt. Seismic profiles suggest that the lower succession is a LST and the upper a likely HST, with the silt reflecting the TST and MFS. Benthic foraminifera indicate paleodepths of 75–80 m at the base and ~75–120 m upsection. The m5.3 sequence is dated as 16.0–15.8 Ma with a 1.6 m.y. hiatus associated with the basal sequence boundary (17.6–16.0 Ma).

Sequence m5.2

At Site M27, the basal m5.2 sequence boundary is placed at a heavily burrowed lithologic contact with apparent rip-up clasts at 236.15 mcd (313–27–83R-2, 129 cm; Fig. 5; Fig. S19 in the Supplemental File [see footnote 1]), separating medium-coarse glauconitic quartz sand above from clay below. It is associated with a sharp gamma-log uphole decrease and sharp

impedance contrast (Fig. 5). Synthetic seismograms place the m5.2 seismic sequence boundary slightly below this (240 mcd, purple arrow Fig. 5), possibly because SMT filters the sharp impedance contrast, smearing it and the reflector over a finite distance. The m5.2 sequence (236.15–225.45 mcd) is in a topset setting at Site M27 (Fig. 2); hence we interpret the upsection facies change from a basal quartz sand to a medial clay yielding deeper water foraminifera (25–80 m paleodepth) to an upper quartz sand as reflecting a TST, MFS, and thin truncated HST. It is dated as 15.0–14.8 Ma, with 0.6 m.y. hiatus associated with the basal sequence boundary.

At Site M28, the basal m5.2 sequence boundary is placed at 323.23 mcd (313–28–38R-2, 106 cm; Fig. 9; Fig. S20 in the Supplemental File [see footnote 1]) at the top of glauconitic sandstones and gravels and a major downhole gamma-log decrease. There is a large impedance contrast at this level due to the high densities below (Fig. 9). The sequence (323.23–276.81 mcd) was drilled immediately landward of the rollover of the underlying sequence. The coarsening-upward sediments above ~310 mcd indicate shallowing upsection from offshore to shoreface-offshore-transition to a channel fill and are clearly the HST. We place the MFS at ~320 mcd at a mud maximum. We interpret the facies from 323.23 to 320 mcd as a TST that fines and deepens upsection. The m5.2 sequence is dated as 15.1–14.8 Ma at this site, with a 0.6 m.y. hiatus associated with the basal sequence boundary.

Site M29 sampled sequence m5.2 on a foreset just seaward of its maximum thickness (Figs. 2 and 16). The basal sequence boundary is placed at 602.25 mcd (313–29–161R-2, 39 cm; Fig. 16; Fig. S21 in the Supplemental File [see footnote 1]) at a contact between clayey silt above and a quartzose glauconite sand below. There is a large impedance contrast at this level and synthetic seismograms place seismic sequence boundary m5.2 precisely at this level. The sequence (602.25–502.01 mcd) was deposited in middle neritic (75–100 m) depths along the foreset of the clinoform and the facies are different than noted in the bottomsets, consisting primarily of fine sandy silts (Fig. 16; Mountain et al., 2010). Subtle grain-size variations may be used in concert with the seismic profiles to interpret surfaces and systems tracts (see summary in Miller et al., 2013b). A coarsening-upward package (602–593 mcd) is interpreted as the LST with TS at its top. The MFS is placed at ~581 mcd at a mud peak, the generally coarsening-upward section above this is interpreted as an HST with 4 parasequences bounded by FS. The m5.2 sequence is dated at Site M29 as 15.6–14.6 Ma with a short (0.2 m.y.) hiatus (15.8–15.6 Ma) associated with the basal sequence boundary.

Sequence m5

At Site M27, the m5 basal sequence boundary is placed at 225.45 mcd (313–27–80R-1, 9 cm; Fig. 5; Fig. S22 in the Supplemental File [see footnote 1]) at a sharp contact at the base of a pebbly, very coarse sand lag and gamma-log minimum. There is a 2.06 m coring gap that limits the interpretation of core impedance data. Interpolation through this gap yields a synthetic seismogram placement of sequence m5 near this level (purple arrow, Fig. 5). This thin, truncated sequence fines upsection, deepening from shoreface to offshore (Fig. 5) and is interpreted to represent a TST. Benthic foraminifera indicate paleodepths were ~25–50 m. It is dated as 13.7–13.6 Ma, with a 1.1 m.y. hiatus across the basal sequence boundary.

At Site M28, the m5 basal sequence boundary is placed at 276.81 mcd (313–28–21R-2, 79 cm; Fig. 9; Fig. S23 in the Supplemental File [see footnote 1]) at top of an indurated zone with gravel-rich sands above and at a major impedance contrast associated with a density maximum. The sequence, deposited on a topset, was not well recovered but the gamma log clearly shows it coarsens upsection; we interpret this as an HST, with both the MFS and TS merged with the sequence boundary. Foraminifera were found only near the base of the sequence, indicating ~10–25 m paleodepth. The m5 sequence is dated as 13.7–13.5 Ma at Site M28, with a 1.1 m.y. hiatus associated with the basal sequence boundary.

At Site M29, the m5 basal sequence boundary is placed at 502.01 mcd (313–29–126R-2, 80 cm; Fig. 15; Fig. S24 in the Supplemental File [see footnote 1]) at a contact of debrite sands above with shoreface sands below. There is only a minor impedance contrast associated with the contact and the synthetic seismograms place the m5 seismic sequence boundary higher (488 mcd) at the base of a clay and a slightly higher impedance contrast (Fig. 15). We cannot resolve this discrepancy, but the major sedimentary facies shift (from shoreface sand to debrite) and associated deepening across the contact is likely the sequence boundary. The m5 sequence (502.01–478.61 mcd) at Site M29 consists of two coarsening-upward successions deposited on a truncated lower foreset to bottomset. The m5 sequence is dated at this site as 13.7–13.6 Ma, with a 0.9 m.y. hiatus associated with the basal sequence boundary (14.6–13.7 Ma).

Sequence m4.5

At Site M27, the m4.5 basal sequence boundary is placed at 218.39 mcd (313–27–75X-2, 68 cm; Fig. 5;. S25 in the Supplemental File [see footnote 1]) at the base of a granuliferous sand abruptly overlying a silty clay, with gravel burrowed down into the silt. At this level there is also a strong impedance contrast and synthetic seismograms place the m4.5 seismic sequence boundary precisely at this level (Fig. 5, Table 1). The sequence (218.39–209 mcd) is located in a topset location at Site M27 and coarsens upward above ~217 mcd indicating an HST (Fig. 5). It is dated as 13.5–13.2 Ma at this site, with a possible short hiatus (~13.6–13.5 Ma) at the basal sequence boundary.

At Site M28, the m4.5 basal sequence boundary is placed at 254.23 mcd (313–28–12R-1, 40 cm; Fig. 9; Fig. S26 in the Supplemental File [see footnote 1]) at a lithologic contact of clayey silts above and medium- to coarse-grained sands below. This level is an impedance contrast. The sequence (254.23–244.16 mcd) is deposited on the topset and consists of a lower silt that deepens upsection (TST), a possible MFS in offshore clays at ~248 and an upper sand indicating a thin HST truncated by the concatenated m4.4-m4.1 sequence boundary (Fig. 9). Sequence m4.5 is dated as 13.3–13.2 Ma at Site M28; there is a short hiatus (0.2 m.y.) associated with the basal sequence boundary.

At Site M29, the m4.5 basal sequence boundary is placed at 478.61 mcd (313–29–118R-1, 25 cm; Fig. 15; Fig. S27 in the Supplemental File [see footnote 1]) at a contact of fine sand above and sandy silt below associated with a 57-cm thick burrowed zone and a large gamma-log increase downsection. This surface was originally correlated to seismic sequence boundary m5 (Mountain et al., 2010), but the revised velocity-depth function indicates correlation to seismic sequence boundary m4.5 (Table 1). There is a very large impedance contrast at this contact and synthetic seismograms place seismic sequence boundary m4.5 precisely at this level (Fig. 15). The sequence (478.61–408.65 mcd) consists of a lower coarsening-upward regressive LST succession to 469 mcd (TS), a fining-upward TST to an MFS at ~448 mcd, and a thick silty HST (Fig. 15). The LST is characterized by transported shallow-water benthic foraminifera (10–25 m; Katz et al., 2013). Within the TST (469–448 mcd), benthic foraminifera indicate a deepening upward from ~40–50 m to ~75–100 m. Much of the HST yields few or no benthic foraminifera below 413.50 mcd; abundant foraminifera from 413.50 to 410.80 indicate 50–80 m paleodepth, with a shallowing at the top of the sequence (25–50 m, 408.90 mcd). The m4.5 sequence is dated as 13.6–13.3 Ma and was deposited at very high sedimentation rates (>200 m/m.y.) with no discernable hiatus at its base. Sequences m4.4, m4.3, m4.2, and m4.1 merge landward of Site M29, and only sequence m4.1 occurs at Sites M27 and M28 (Fig. 2).

TABLE 1. DEPTH, AGES, TWO-WAY TRAVELTIME, SYNTHETIC SEISMOGRAM DEPTH, AND IMPEDANCE CONTRASTS

Site M27						Site M28					Site M29					
Sequence	Depth (mcd)	Age (Ma)	TWT (msecs bsf)	Synthetic (mcd)	Impedance contrast	Sequence	Depth (mcd)	Age (Ma)	TWT (msecs bsf)	Impedance contrast	Sequence	Depth (mcd)	Age (Ma)	TWT (msecs bsf)	Synthetic (mcd)	Impedance contrast
	0	0.072														
uP3	13.57	0.085	15	NR	NR											
	13.57	0.19														
uP1	21.42/22.8	0.22	31	NR	NR											
	21.42/22.8	1.03?														
*IP2	26.4	1.08?	NR	NR	NR											
	26.4	1.4?														
*IP1	31.9	1.5?	NR	NR	NR											
	31.9															
m1	96	NR	161	NR	NR											
	96															
m3	111	NR	182	NR	NR											
	111															
m4	135	NR	211	NR	NR											
	135												?12.6			
m4.1	209		288	210	yes	m4.1	244.16	?	333		m4.1	343.81	13	437	NR	yes
												343.81	13			
											m4.2	364.86	13.1	460	NR	yes
												364.86	13.1			
											m4.3	377.15	13.2	471	NR	?
												377.15	13.2			
											m4.4	409.27	13.3	510	411	yes
	209	13.2					244.16	13.2				409.27	13.3			
m4.5	218.39	13.5	296	218	yes	m4.5	254.23	13.3	344	yes	m4.5	478.61	13.6	568	478	yes
	218.39	13.6					254.23	13.5				478.61	13.6			
m5	225.45	13.7	298	222	yes	m5	276.81	13.7	366	yes	m5	502.01	13.7	597	488	?
	225.45	14.8					276.81	14.8				502.01	14.6			
m5.2	236.15	15	320	240	yes	m5.2	323.23	15.1	423	yes	m5.2	602.25	15.6	710	602	yes
	236.15	15.6					323.23	15.7				602.25	15.8			
m5.3 alt.	249.76		336	NR	no											
m5.3	256.19	15.8	336	NR	yes	m5.3	361.0	16.3	458	NR	m5.3	643.19	16.0	754	648	yes

(*continued*)

TABLE 1. DEPTH, AGES, TWO-WAY TRAVELTIME, SYNTHETIC SEISMOGRAM DEPTH, AND IMPEDANCE CONTRASTS (*continued*)

Site M27					
Sequence	Depth (mcd)	Age (Ma)	TWT (msecs bsf)	Synthetic (mcd)	Impedance contrast
	256.19	16.5			
m5.33	271.23	16.6		NR	yes
	271.23	16.9			
m5.34	295.01	17.0	382	295	yes
m5.4-1	cut out			NR	
	295.01	17.7			
m5.45	336.06	18	432	NR	no
	336.06	?			
m5.47	355.53	?	446	NR	NR
	X				
m5.6	X		cut out		
	355.53	?			
m5.7	361.28	?	458	NR	NR
	361.28	19.2			
m5.8	494.87	20.1	591	493	yes
	494.87	20.7			
m6	509/515	20.9	607	?510	yes
	509/515	23			
*O6	538.68	23.5	NR	NR	NR
	538.68	28.2			
*O3	617	29.3	NR	NR	NR
	617	32.2			
*O1	625.83	32.3	NR	NR	NR

Site M28				
Sequence	Depth (mcd)	Age (Ma)	TWT (msecs bsf)	Impedance contrast
	361.0	16.6		
m5.33	405.0	16.7		NR
	405.0	17.4		
m5.34	479.0	17.6		?
	479.0	17.6		
m5.4-1	512.33	17.7	612	?
	512.33	17.9		
m5.45	533.59	18.0	633	yes
	533.59	?		
m5.47	545.5	?	646	?
	545.5	?		
m5.6	567.5	?	666	yes
	567.5	18.6		
m5.7	611.6	18.8	710	yes
	611.6	19.5		
m5.8	662.98	20.0	772	?

Site M29					
Sequence	Depth (mcd)	Age (Ma)	TWT (msecs bsf)	Synthetic (mcd)	Impedance contrast
	643.19	17.6			
m5.4	662.37	17.7	769	661	yes
	662.37	17.7			
m5.45	673.71	17.8	768		yes (negative)
5.45 alt.	683.17		768	681	yes
	673.71	17.9			
m5.45 alt.	683.17				
m5.47	687.87	18.0	798		?
m5.47 alt.	695.65		798	696	?
	687.87	18.1			
m5.47 alt.	695.65				
m5.6	707.56/710	18.3	825	>715	NR
	707.56/710	18.6			
m5.7	728.56	18.8	849		NR
	728.56	20.0			
m5.8	746	20.2	860		NR

Note: NR—not resolved; mcd—meters composite depth; bsf—below seafloor; TWT—two-way traveltime.
*Not resolved on seismic profiles.

Sequence m4.4

The basal m4.4 sequence boundary occurs at Site M29 within a monotonous silt and silty clay succession. We tentatively place the lithologic sequence boundary at a heavily bioturbated surface at 409.27 mcd (313–29R-94–1, 106 cm; Fig. 15; Fig. S28 in the Supplemental File [see footnote 1]), although it is possible to place it at an irregular surface separating clay from silt at 409.63 mcd (313–29R-94–1, 142–144 cm). There is an impedance contrast at this level and synthetic seismograms indicate correlation of seismic sequence boundary m4.4 to this level (Supplemental Table [see footnote 2]). This site sampled the sequence on a truncated foreset (paleodepth 50–80 m, with some barren samples) where it consists of silt and silty clay capped by a few sand beds. The sequence (409.27–371.15 mcd) is dated as ~13.3–13.2 Ma, indicating that it was deposited at very high sedimentation rates (>300 m/m.y.).

Sequence m4.3

The basal m4.3 sequence boundary is tentatively placed at 377.15 mcd (313–29–83R-2, 99 cm; Fig. 15; Fig. S29 in the Supplemental File [see footnote 1]) at the base of a shelly sand lying on silty clays at an upsection increase in gamma-log values. This highly truncated sequence is only approximately dated as 13.2–13.1 Ma, with no discernable hiatus at the basal sequence boundary.

Sequence m4.2

The basal m4.2 sequence boundary at Site M29 is tentatively placed at 364.86 mcd (313–29–79R-2, 90 cm; Figs. 14 and 15; Fig. S30 in the Supplemental File [see footnote 1]) at the base of a graded bed separating sands above from silty clays below. There is an impedance contrast at this level; no synthetic seismogram data are available. The section from 364.86 to 342.81 mcd consists of two coarsening-upward successions that appear to be parasequences; benthic foraminifera in the first succession indicate 25–50 m paleodepth, but are absent from the second succession. The sequence is sampled landward of the clinoform rollover, although erosion associated with the lower sequence boundary suggests this may be a LST, an interpretation consistent with coarsening-upward parasequences. The m4.2 succession is tentatively dated as 13.1–13.0 Ma.

Sequence m4.1

At Site M29, the m4.1 sequence boundary is placed at 343.81 mcd (313–29–72R-1, 49 cm; Fig. 14) in an indurated interval at an irregular surface separating silty clays above from fine sand below associated with a gamma-log increase and a sharp impedance contrast (no synthetic seismogram data are available). This level is a major impedance contrast (Fig. 14). The sequence boundary is likely merged with the TS. The sequence consists of a thin TST with an MFS at ~340–335 mcd based on maximum water depths indicated by benthic foraminifera, and a thick HST that extends above 280 mcd where coring began. Benthic foraminiferal assemblages support this interpretation, indicating paleodepths of 75–100 m above reflector m4.1 (338.81–335.76 mcd). The rest of the sequence sampled (to ~255 mcd) is a regressive HST, with shallower assemblages (334.23 mcd, 40–60 m; 332.71 mcd, 25–50 m) overlain by barren samples. The top sequence boundary was not sampled. Seismic interpretations predict the m4 seismic sequence boundary at 242 mcd in an uncored interval. The m4.1 succession is poorly dated as ~13.0–12.6 Ma by extrapolation, although the top of the sequence was not cored.

The m4.1–4.4 concatenated sequence boundary occurs at 209 mcd at Site M27 (Fig. 4) and 244.16 mcd (313–28–8-2, 103 cm) at Site M28 (Fig. 9; Fig. S31 in the Supplemental File [see footnote 1]). At Site M27 the m4.1–4.4 sequence consists of a thick clay to 183 mcd that coarsens upsection to a medium-coarse sand (Fig. 4); the overlying sequence boundary was spot cored at ~135 mcd. At Site M28, the m4.1–4.4 concatenated sequence boundary is a sharp (±1–2 cm) contact of laminated clay on a medium, shelly sand. The top was not sampled. It is poorly dated as younger than 13.2 Ma.

Sequences Younger Than m4.1

Three upper middle Miocene sequence boundaries (m4, m3, and m1; Miller et al., 1998) were traced to their far updip topset position and spot cored at M27 and M29. Limited facies information was gained, although the m4 sequence appears to be a fluvial delta plain deposit and sequence boundary m3 appears to be associated with a paleosol (Fig. 13) at Site M29. The m1 sequence appears to be fluvial estuarine at Site M27 (Fig. 3). The placement of the m3 and m1 sequence boundaries at Site M29 from the velocity-depth function (Fig. 13) are within 2 and 6 m, respectively of major gamma-log upsection increases, and these are the likely the placement of the sequence boundaries. No age information is available for these sequences except they appear to be younger than ~13.0 Ma. This slightly conflicts with ages of m4 (older than 13.6 Ma) and m3 (13.6 Ma) dated on the slope (Miller et al., 1998), but this time correlation requires updating. For a discussion of the revised age relations of the age relations of upper middle Miocene sequence boundaries m4, m3, and m1, see Browning et al. (2013).

DISCUSSION

Placement of Sequence Boundaries

The fundamental first step in applying sequence stratigraphy is to recognize sequence-bounding unconformities. Although maximum flooding surfaces are also important (Galloway, 1989) and stacking patterns informative (Van Wagoner et al., 1990), unequivocal recognition of sequence boundaries provides the building blocks of the sequence stratigraphic record. Many sequence boundaries are subtle and their criteria are lacking. Expedition 313 (Mountain et al., 2010) first examined the split cores in Bremen in 2009 and used an iterative approach to identify of sequence boundaries, following these steps in initial seismic-core-log correlations:

1. Sequence boundaries were recognized on seismic profiles using classic criteria, traced, and loop correlated through the seismic grid (Monteverde et al., 2008; Monteverde, 2008; Mountain et al., 2010).

2. Candidate sequence boundaries, MFS, and TS were recognized by sedimentologists in cores and by the loggers in downhole and MSCL core logs (Mountain et al., 2010).

3. The depths of seismic sequence boundaries were predicted with the initial velocity-depth function.

4. The stratigraphic correlators took the predicted placement from seismic profiles and the initial placement of the sequence boundaries in the cores and integrated with teams that evaluated the lithostratigraphy (grain size, mineralogy, facies, and paleoenvironments), facies successions, benthic foraminiferal water depths, downhole and core gamma logs (especially gamma and impedance), and chronostratigraphic ages (Mountain et al., 2010). The best estimate was indicated on a series of figures that formed the basis of the progenitors of Figures 3–17 shown here (e.g., figs. F65–69 of Site M27 in Mountain et al., 2010).

This study includes several new data sets not available in Bremen including: quantitative lithology, much more detailed age and benthic foraminiferal data, and a new velocity-depth function (Figs. 3–17) that improve our recognition of sequence boundaries in cores. The revised velocity-depth function shifted the depths of a few sequence boundaries relative to the core and log surfaces; although it improved the fit, the revised correlation raises the questions, how reliable are the correlations of the seismic sequence boundaries to the core and log expression of sequence boundaries? How many

(if any) of the correlations presented here are spurious?

The generation of synthetic seismograms (Mountain and Monteverde, 2012) provides a high degree of confidence that we can successfully match most core and log surfaces unequivocally with seismic sequence boundaries. Synthetic seismograms successfully link seismic sequence boundaries to their equivalent core sequence boundary in 7 of 12 cases at Site M27 and 9 of 14 cases at Site M29 (Table 1), most within 1 m of the prediction and all within 5 m. However, in spite of the availability of a nearly optimum set of constraints, comprising high-quality seismic profiles, continuous cores and downhole logs from a transect of three coreholes spanning clinothems in topset, foreset, and bottomset locations, uncertainties remain as outlined in the Results discussion section. Future improvement of seismic imaging by 3-D profiling would resolve many of these ambiguities. Nevertheless, our efforts provide a sequence stratigraphic framework for other Expedition 313 studies, allowing site to site physical correlation and evaluation of facies changes within sequences (e.g., systems tracts, faunal successions, log expressions; see Miller et al., 2013b). Our sequence stratigraphic framework is also a vital prerequisite to one-dimensional and two-dimensional backstripping to reconstruct margin evolution and provide eustatic estimates.

This study shows that seismic reflections below m6 are Oligocene (o.1 and o.5), but do not correlate with sequence boundaries. This is for several reasons: 1) the degraded quality of pre-Miocene seismic resolution due to either increasing burial depth or less stratal organization; and 2) the lack of reflector terminations visible on our profiles. Previous studies have interpreted Oligocene reflector terminations and sequence boundaries (e.g., Greenlee and Moore, 1988). These may in fact be real on adjacent seismic profiles where the Oligocene is thicker, but cannot be verified on Line 529 (Fig. 2).

Significance of Sequence Boundaries

Excellent recovery of Miocene sequences allows core-seismic integration that confirms the hypothesis that sequence-bounding unconformities are a primary source of major impedance contrasts in reflection seismic data. Miocene sequence boundaries correspond well with impedance contrasts (Table 1). Data quality are sufficient to link sequence boundaries to impedance contrasts in 9 of 12 instances at Sites M27, 6 of 11 instances at M28, and 8 of 14 instances at M29 (Table 1). In all cases but one, the lack of an impedance contrast is due to a data gap. The exception is m5.45 at Site M27 (Fig. 6), which should be a major impedance contrast associated with a change from clays above to granuliferous sands below (Fig. S8); we attribute this to poor MSCL velocity logs from the sand (no downhole velocity log is available for this section) and data gaps.

Other stratal surfaces also yield impedance contrasts. For example, impedance contrast are associated with:

1) FS at ~323 and ~308 mcd in sequence m5.45 at Site M27 (Fig. 6);

2) an MFS at 442 mcd in sequence m5.8 at Site M27 (Fig. 7);

3) a possible MFS at 505 mcd on a bottomset in sequence m6 at Site M27 (Fig. 8);

4) an MFS at 494 mcd within sequence m5.4 at Site M28 (Fig. 10);

5) an MFS at 448 mcd in sequence m4.5 at Site M29 (Fig. 15); and

6) FSs within m5.2 at Site M29 (Fig. 16).

Several sediment facies boundaries also appear to be associated with impedance contrasts, almost exclusively those on bottomsets going from sands below to clays above. These include the following at Site M29: 490 mcd (Fig. 15), ~625 mcd (Fig. 16), and 681 mcd (Fig. 17). These may be FS on the bottomsets, although the facies model for deposits on the bottomsets is complex (Mountain et al., 2010). Intrasequence O3 reflectors o.1 and o.5 at Site M27 (Fig. 8) are associated with facies changes on bottomsets. One change in impedance contrast not on a bottomset that may be associated with a facies change occurs in sequence m5.8 at Site M27 at ~470 m where a gradual upsection decrease in impedance is associated with a gradual fining upsection in the TST (Fig. 7).

Synthetic seismograms confirm that sequence boundaries are major reflections, although other stratal surfaces (e.g., MFS, TS, and FS) also produce prominent reflections. The only conflicts between correlations by the synthetic seismogram and core placement are on the bottomsets at Site M29 (sequence boundaries m5.45 and 5.47, where the synthetic seismograms place the major reflections at what we interpreted as abrupt facies changes from sands below to clays above [Fig. 17]). The key conclusion is that bottomset facies changes are sharp and yield impedance contrasts, and further studies of these bottomsets and their stratal surfaces are needed. There are other possible impedance contrasts, but the data collected by Expedition 313 was limited by poor log quality in some sandy sections that precludes further testing (= NR on Table 1). Nevertheless, it is clear that sequence-bounding unconformities are the primary source of impedance contrasts at our sites (Table 1), with MFS and FS also yielding impedance contrasts.

The causes of the impedance contrasts vary. Of the 23 confirmed links between sequence boundaries and impedance contrasts (Table 1), 8 have muds over sands, 10 have sands over muds, 2 have sands over sands, and 3 are indurated zones. Lithologic contacts (e.g., muds over sands or vice versa) do not necessarily always generate significant impedance contrasts, especially those contacts that are gradational (e.g., coarsening upward in HST like sequence m5.2 at Site M28 where the change occurs over a 5-m interval; Fig. 9). Although seismic reflectors often result from convolution of the wavelet over several meters (e.g., New Jersey slope Site 904, where seismic sequence boundary m6 is associated with a ~5 m thick impedance contrast; Miller et al., 2005), the impedance contrasts associated with major seismic sequence boundaries at Sites M27–M29 are relatively sharp (~1–2 m). These sharp contrasts can result from abrupt lithofacies shifts associated with sequence boundaries; however, most sequence boundaries show extensive bioturbation suggesting short time gaps (diastems) with differential compaction below and above, suggesting that lithology is not the primary cause of the contrast.

Expression of Sequence Boundaries and Facies Changes in Different Settings

The primary purpose of this paper is to recognize and discuss the seismic significance sequence boundaries. Other papers on Expedition 313 will discuss facies changes within sequences. To consider fully the placement of sequence boundaries, some attention is needed to fining- and/or coarsening-upward trends and stacking patterns, with their implications to systems tracts. We have not fully interpreted systems tracts here, particularly on bottomsets, but provide some comments on the nature of sequence boundaries in different clinothem settings and with respect to systems tracts.

Sequence boundaries were sampled on topsets, foresets, and bottomsets (including far updip topsets in the onshore coreholes). Oligocene sequences were only sampled at Site M27 and have minimal sequence and seismic expression due to basinal locations. Miocene sequence boundaries on the topsets have clear lithologic expression and often consist of TST clays sitting on HST sands of the underlying sequence (e.g., m4.1, m4.5, m5 at Site M27, m4.5, m5.2 at Site M28), although this pattern is more complicated and less predictable than far updip at onshore sites (e.g., TST sand sit on TST clays at m5.2 at Site M27). Drilling on the foresets (m5.8 at Site M27, M5.4 at Site M28, and m5.2 at Site M29; Fig. 2) yields complete sequences with

LST, TST, and HST; the basal sequence boundaries on foresets are recognizable, even though they stack coarsening-upward HST on coarsening-upward LST (Figs. 7, 10, and 16). We also drilled on the foresets of the 4.5 and m4.4 sequences, though seismically it appears that these are truncated and thus are not as thick and stratigraphically complete (Fig. 2). Recognition of sequence boundaries on bottomsets is more difficult as discussed above.

The correlative conformity has not been identified in the Expedition 313 coreholes, though seismic criteria suggest we sampled across seismically recognized conformities. Two positions on a clinothem have been inferred to have possible correlative conformities on the Miocene of the New Jersey shelf: the foresets and the bottomsets (fig. 2 in Greenlee and Moore, 1988). We show that in foresets, where sequences are thickest and presumably most complete, there is evidence of erosion and hiatuses associated with sequence boundaries. For example, sequence boundary m5.2 at Site M29 sampled a foreset where the boundary appears seismically conformable (Fig. 2) (see Fig. 10 in Miller et al., 2013b), yet a physical break is observed (Fig. S21) and short hiatus inferred (15.8–15.6 Ma). Similarly, the contact of sequence m5.8 and m6 is seismically conformable in the foreset at Site M27 (Fig. 2) (see Fig. 10 in Miller et al., 2013b), but there is a distinct break (Fig. S4) and hiatus from 20.7 to 20.1 Ma. We also show that continuity does not occur on the bottomsets (e.g., sequence boundary m5.8 at Site M29 has a 0.3 m.y. hiatus). Though there are several sequence boundaries with no discernible time gaps (Table 1, Browning et al., 2013), there is still evidence of erosion associated with sequence boundaries, even in bottomsets. In general, in the shallow (<100 m paleodepth) shelf, we see little evidence for a correlative conformity. Certainly tracing seismic reflectors into deep water (>200–2000 m), sections can approach continuity, though even here downslope processes can erode sequences boundaries. An excellent example of this is provided at New Jersey slope Site 904 (1123 m present depth, ~1000 m paleodepth), where six lower Miocene sequence boundaries are associated with only 4 confirmed hiatuses (Miller et al., 1998, 2005). Future work is needed to correlate firmly these lower Miocene sequence boundaries from the slope to the Expedition 313 area.

CONCLUSIONS

In this study, we have integrated a diverse and comprehensive number of seismic (profiles, velocity-depth, and synthetic seismograms), core (surfaces, lithology including grain size, mineralogy, facies, and paleoenvironments, facies successions, benthic foraminiferal water depths, and chronostratigraphic ages), and log (downhole and core gamma logs and velocity and core density) data sets to provide a clear (if not unequivocal in many cases) sequence stratigraphic framework for the uppermost Eocene to lower middle Miocene of the New Jersey shallow shelf. Several generations of multichannel seismic profiles allow seismic recognition of 15 early to early-middle Miocene seismic sequence boundaries that here are tied to impedance contrasts in the cores. Synthetic seismograms confirm the placement of seismic sequence boundaries with core and log data and the hypothesis that seismic disconformities are a primary cause of seismic reflections on shallow shelves. The causes of impedance contrasts are varied and depend on their location on the topset, foreset, or bottomsets of clinothems. This study affirms the fundamental unit and principle of sequence stratigraphy, that sequence bounding unconformities are recognizable in seismic profiles, cores, and well logs, and that any study employing sequence stratigraphy should begin with identification of sequence boundaries.

ACKNOWLEDGMENTS

We thank the drillers and scientists of Expedition 313 for their enthusiastic collaboration, the Bremen Core Repository for hosting our studies, C. Lombardi, J. Criscione, and R. Miller for lithologic analyses, V. Abreu for discussions of construction of the Exxon curve, and P. Sugarman and S. Karakaya for discussions. Funding was supplied by the Consortium for Ocean Leadership/U.S. Science Support Program (COL/USSP) and samples provided by the Integrated Ocean Drilling Program and the International Continental Scientific Drilling Program. We thank D. Hodgson, T.C. Moore, and an anonymous reviewer for comments.

REFERENCES CITED

Abreu, V., Neal, J.E., Bohacs, K.M., and Kalbas, J.L., 2010, Sequence stratigraphy of siliciclastic systems—The ExxonMobil methodology atlas of exercises: SEPM (Society for Sedimentary Geology) Concepts in Sedimentology and Paleontology 9, 226 p.

Ager, D.V., 1973, The nature of the stratigraphical record: New York, John Wiley, 114 p.

Austin, J.A., Christie-Blick, N., Malone, M., and the Leg 174A Shipboard Party, eds., 1998, Proceedings of the Ocean Drilling Program, Initial reports, Volume 174A: College Station, Texas, Ocean Drilling Program, doi: 10.2973/odp.proc.ir.174a.1998.

Ball, M.M., and 14 others, 1992, Ocean Drilling Program guidelines for pollution prevention and safety: JOIDES Journal, v. 18, special issue 7, p. 1–24.

Browning, J.V., Miller, K.G., McLaughlin, P.P., Kominz, M.A., Sugarman, P.J., Monteverde, D., Feigenson, M.D., and Hernàndez, J.C., 2006, Quantification of the effects of eustasy, subsidence, and sediment supply on Miocene sequences, Mid-Atlantic margin of the United States: Geological Society of America Bulletin, v. 118, p. 567–588, doi:10.1130/B25551.1.

Browning, J.V., Miller, K.G., Sugarman, P.J., Barron, J., McCarthy, F.M.G., Kulhanek, D.K., Katz, M.E., and Feigenson, M.D., 2013, Chronology of Eocene–Miocene sequences on the New Jersey shallow shelf: Implications for regional, interregional, and global correlations: Geosphere, doi:10.1130/GES00857.1.

Catuneanu, O., 2006, Principles of sequence stratigraphy: Amsterdam, Elsevier, 375 p.

Christie-Blick, N., 1991, Onlap, offlap, and the origin of unconformity-bounded depositional sequences: Marine Geology, v. 97, p. 35–56, doi:10.1016/0025-3227(91)90018-Y.

Christie-Blick, N., and Driscoll, N.W., 1995, Sequence stratigraphy: Annual Review of Earth and Planetary Sciences, v. 23, p. 451–478, doi:10.1146/annurev.ea.23.050195.002315.

Christie-Blick, N., Mountain, G.S., and Miller, K.G., 1990, Seismic stratigraphic record of sea level change, *in* Geophysics Study Committee, National Research Council, Sea-level change: National Academy of Sciences Studies in Geophysics: Washington, D.C., National Academy Press, p. 116–140.

Deptuck, M.E., Sylvester, Z., Primez, C., and O'Byrne, C., 2007, Migration-aggradation history and 3-D seismic geomorphology of submarine channels in the Pleistocene Benin-Major Canyon, western Niger Delta slope: Marine and Petroleum Geology, v. 24, p. 406–433, doi:10.1016/j.marpetgeo.2007.01.005.

Embry, A.F., 2009, Practical sequence stratigraphy: Canadian Society of Petroleum Geologists, 81 p., www.cspg.org.

Fulthorpe, C.S., and Austin, J.S., Jr., 2008, Assessing the significance of along-strike variations of middle to late Miocene prograding clinoformal sequence geometries beneath the New Jersey continental shelf: Basin Research, v. 20, p. 269–283, doi:10.1111/j.1365-2117.2008.00350.x.

Galloway, W.E., 1989, Genetic stratigraphic sequences in basin analysis I: Architecture and genesis of flooding-surface bounded depositional units: American Association of Petroleum Geologists Bulletin, v. 73, p. 125–142.

Greenlee, S.M., and Moore, T.C., 1988, Recognition and interpretation of depositional sequences and calculation of sea level changes from stratigraphic data—Offshore New Jersey and Alabama Tertiary, *in* Wilgus, C.K., et al., eds., Sea-level changes: An integrated approach: SEPM (Society of Economic Paleontologists and Mineralogists) Special Publication 42, p. 329–353.

Greenlee, S.M., Devlin, W.J., Miller, K.G., Mountain, G.S., and Flemings, P.B., 1992, Integrated sequence stratigraphy of Neogene deposits, New Jersey continental shelf and slope: Comparison with the Exxon model: Geological Society of America Bulletin, v. 104, p. 1403–1411, doi: 10.1130/0016-7606(1992)104<1403:ISSOND>2.3.CO;2.

Haq, B.U., Hardenbol, J., and Vail, P.R., 1987, Chronology of fluctuating sea levels since the Triassic (250 million years ago to present): Science, v. 235, p. 1156–1167, doi:10.1126/science.235.4793.1156.

Hathaway, J.C., Poag, C.W., Valentine, P.C., Miller, R.E., Schultz, D.M., Manheim, R.T., Kohout, F.A., Bothner, M.H., and Sangrey, D.A., 1979, U.S. Geological Survey core drilling on the Atlantic shelf: Science, v. 206, p. 515–527, doi:10.1126/science.206.4418.515.

John, C.M., Karner, G.D., and Mutti, M., 2004, $\delta^{18}O$ and Marion Plateau backstripping: Combining two approaches to constrain late middle Miocene eustatic amplitude: Geology, v. 32, p. 829–832, doi:10.1130/G20580.1.

John, C.M., Karner, G.D., Browning, E., Leckie, M., Mateo, Z., Carson, B., and Lowery, C., 2011, Timing and magnitude of Miocene eustasy derived from the mixed siliciclastic-carbonate stratigraphic record of the northeastern Australian margin: Earth and Planetary Science Letters, v. 304, p. 455–467, doi:10.1016/j.epsl.2011.02.013.

Katz, M.E., Browning, J.V., Miller, K.G., Monteverde, D., Mountain, G.S., and Williams, R.H., 2013, Paleobathymetry and sequence stratigraphic interpretations 1 from benthic foraminifera: Insights on New Jersey shelf architecture, IODP Expedition 313: Geosphere, doi:10.1130/GES00872.1 (in press).

Kominz, M.A., Miller, K.G., and Browning, J.V., 1998, Long-term and short-term global Cenozoic sea-level estimates: Geology, v. 26, p. 311–314, doi:10.1130/0091-7613(1998)026<0311:LTASTG>2.3.CO;2.

Kominz, M.A., Van Sickel, W.A., Miller, K.G., and Browning, J.V., 2002, Sea-level estimates for the latest 100 million years: One-dimensional backstripping of onshore New Jersey boreholes, *in* Armentrout, J., and Rosen, N., eds.,

Sequence stratigraphic models for exploration and production: Evolving methodology, emerging models, and application case histories: Proceedings, 22nd Annual GCSSEPM Foundation Bob F. Perkins Research Conference, p. 303–315.

Kominz, M.A., Browning, J.V., Miller, K.G., Sugarman, P.J., Misintseva, S., and Scotese, C.R., 2008, Late Cretaceous to Miocene sea-level estimates from the New Jersey and Delaware coastal plain coreholes: An error analysis: Basin Research, v. 20, p. 211–226, doi: 10.1111/j.1365-2117.2008.00354.x.

Loutit, T.S., Hardenbol, J., Vail, P.R., and Baum, G.R., 1988, Condensed section: The key to age determination and correlation of continental margin sequences, *in* Wilgus, C.K., et al., eds., Sea-level changes: An integrated approach: SEPM (Society of Economic Paleontologists and Mineralogists) Special Publication 42, p. 183–213.

Miller, K.G., and Mountain, G.S., 1994, Global sea-level change and the New Jersey margin, *in* Mountain, G.S., et al., eds., Proceedings of the Ocean Drilling Program, Initial reports, Volume 150: College Station, Texas, Ocean Drilling Program, p. 11–20, doi:10.2973/odp .proc.ir.150.102.1994.

Miller, K.G., Fairbanks, R.G., and Mountain, G.S., 1987, Tertiary oxygen isotope synthesis, sea level history, and continental margin erosion: Paleoceanography, v. 2, p. 1–19, doi:10.1029/PA002i001p00001.

Miller, K.G., Wright, J.D., and Fairbanks, R.G., 1991, Unlocking the ice house: Oligocene–Miocene oxygen isotopes, eustasy, and margin erosion: Journal of Geophysical Research, v. 96, p. 6829–6848, doi:10.1029 /90JB02015.

Miller, K.G., Mountain, G.S., the Leg 150 Shipboard Party, and Members of the New Jersey Coastal Plain Drilling Project, 1996a, Drilling and dating New Jersey Oligocene–Miocene sequences: Ice volume, global sea level, and Exxon records: Science, v. 271, p. 1092–1095, doi:10.1126/science.271.5252.1092.

Miller, K.G., Liu, C., and Feigenson, M.D., 1996b, Oligocene to middle Miocene Sr-isotopic stratigraphy of the New Jersey continental slope, *in* Mountain, G.S., et al., eds., Proceedings of the Ocean Drilling Program, Scientific results, Volume 150: College Station, Texas, Ocean Drilling Program, p. 97–114, doi:10.2973/odp .proc.sr.150.011.1996.

Miller, K.G., Browning, J.V., Pekar, S.F., and Sugarman, P.J., 1997a, Cenozoic evolution of the New Jersey coastal plain: Changes in sea level, tectonics, and sediment supply, *in* Miller, K.G., and Snyder, S.W., eds., Proceedings of the Ocean Drilling Program, Scientific results, Volume 150X: College Station, Texas, Ocean Drilling Program, p. 361–373, doi:10.2973/odp.proc .sr.150X.326.1997.

Miller, K.G., Rufolo, S., Sugarman, P.J., Pekar, S.F., Browning, J.V., and Gwynn, D.W., 1997b, Early to middle Miocene sequences, systems tracts, and benthic foraminiferal biofacies, New Jersey coastal plain, *in* Miller, K.G., and Snyder, S.W., eds., Proceedings of the Ocean Drilling Program, Scientific results, Volume 150X: College Station, Texas, Ocean Drilling Program, p. 169–186, doi:10.2973/odp.proc.sr.150X.313.1997.

Miller, K.G., Mountain, G.S., Browning, J.V., Kominz, M., Sugarman, P.J., Christie-Blick, N., Katz, M.E., and Wright, J.D., 1998, Cenozoic global sea level, sequences, and the New Jersey transect: Results from coastal plain and slope drilling: Reviews of Geophysics, v. 36, p. 569–601, doi:10.1029/98RG01624.

Miller, K.G., Kominz, M.A., Browning, J.V., Wright, J.D., Mountain, G.S., Katz, M.E., Sugarman, P.J., Cramer, B.S., Christie-Blick, N., and Pekar, S.F., 2005, The Phanerozoic record of global sea-level change: Science, v. 310, p. 1293–1298, doi:10.1126/science.1116412.

Miller, K.G., Mountain, G.S., Wright, J.D., and Browning, J.V., 2011, A 180-million-year record of sea level and ice volume variations from continental margin and deep-sea isotopic records: Oceanography, v. 24, p. 40–53, doi:10.5670/oceanog.2011.26.

Miller, K.G., Sugarman, P.J., Browning, J.V., Sheridan, R.E., Kulhanek, D.K., Monteverde, D., Wehmiller, J.F., Lombardi, C., and Feigenson, M.D., 2013a, Pleistocene sequence stratigraphy of the shallow continental shelf, offshore New Jersey: Constraints of Integrated Ocean Drilling Program Leg 313 core holes: Geosphere, v. 9, p. 74–95, doi:10.1130/GES00795.1.

Miller, K.G., and 13 others, 2013b, Testing sequence stratigraphic models by drilling Miocene foresets on the New Jersey shallow shelf: Geosphere, doi:10.1130 /GES00884.1.

Mitchum, R.M., Jr., and Van Wagoner, J.C., 1991, High-frequency sequences and their stacking patterns; sequence-stratigraphic evidence of high-frequency eustatic cycles: Sedimentary Geology, v. 70, p. 131–160, doi:10.1016/0037-0738(91)90139-5.

Mitchum, R.M., Vail, P.R., and Thompson, S., 1977, The depositional sequence as a basic unit for stratigraphic analysis: American Association of Petroleum Geologists Memoir, v. 26, p. 53–62.

Monteverde, D.H., 2008, Sequence stratigraphic analysis of early and middle Miocene shelf progradation along the New Jersey margin [Ph.D. thesis]: New Brunswick, New Jersey, Rutgers University, 247 p.

Monteverde, D.H., Mountain, G.S., and Miller, K.G., 2008, Early Miocene sequence development across the New Jersey margin: Basin Research, v. 20, p. 249–267, doi: 10.1111/j.1365-2117.2008.00351.x.

Moucha, R., Forte, A.M., Mitrovica, J.X., Rowley, D.B., Quere, S., Simmons, N.A., and Grand, S.P., 2008, Dynamic topography and long–term sea level variations: There is no such thing as a stable continental platform: Earth and Planetary Science Letters, v. 271, p. 101–108, doi:10.1016/j.epsl.2008.03.056.

Mountain, G., and Monteverde, D., 2012, If you've got the time, we've got the depth: The importance of accurate core-seismic correlation: American Geophysical Union Fall Meeting, abstract PP51B-2111.

Mountain, G.S., Miller, K.G., and Blum, P., eds., 1994, Proceedings of the Ocean Drilling Program, Initial reports, Volume 150: College Station, Texas, Ocean Drilling Program, 885 p., doi:10.2973/odp.proc.ir.150.1994.

Mountain, G.S., Proust, J.-N., McInroy, D., and Cotterill, C., and the Expedition 313 Scientists, 2010, Proceedings of the Integrated Ocean Drilling Program, Expedition 313: Tokyo, Integrated Ocean Drilling Program Management International, Inc., doi:10.2204/iodp.proc .313.2010.

Neal, J., and Abreu, V., 2009, Sequence stratigraphy hierarchy and the accommodation succession method: Geology, v. 37, p. 779–782, doi:10.1130/G25722A.1.

Nystuen, J.P., 1998, History and development of sequence stratigraphy, *in* Gradstein, F.M., et al., eds., Sequence stratigraphy—Concepts and applications: Norwegian Petroleum Society Special Publication 8, p. 31–116.

Pekar, S.F., Miller, K.G., and Browning, J.V., 1997, New Jersey Coastal Plain Oligocene sequences, *in* Miller, K.G., and Snyder, S.W., eds., Proceedings of the Ocean Drilling Program, Scientific results, Volume 150X: College Station, Texas, Ocean Drilling Program, p. 186–206, doi:10.2973/odp.proc.sr.150X.314.1997.

Pekar, S.F., Christie-Blick, N., Kominz, M.A., and Miller, K.G., 2001, Evaluating the stratigraphic response to eustasy from Oligocene strata in New Jersey: Geology, v. 29, p. 55–58, doi:10.1130/0091-7613(2001)029 <0055:ETSRTE>2.0.CO;2.

Pekar, S.F., Christie-Blick, N., Kominz, M.A., and Miller, K.G., 2002, Calibration between eustatic estimates from backstripping and oxygen isotopic records for the Oligocene: Geology, v. 30, p. 903–906, doi:10.1130/0091 -7613(2002)030<0903:CBEEFB>2.0.CO;2.

Peltier, W.R., 1998, Postglacial variations in the level of the sea: Implications for climate dynamics and solid-earth geophysics: Reviews of Geophysics, v. 36, p. 603–689, doi:10.1029/98RG02638.

Pitman, W.C., 1978, Relationship between eustasy and stratigraphic sequences on passive margins: Geological Society of America Bulletin, v. 89, p. 1389–1403, doi:10.1130/0016-7606(1978)89<1389:RBEASS>2.0 .CO;2.

Raymo, M.E., Mitrovica, J.X., O'Leary, M.J., DeConto, R.M., and Hearty, P.J., 2011, Departures from eustasy in Pliocene sea-level records: Nature Geoscience, v. 4, p. 328–332, doi:10.1038/ngeo1118.

Rider, M., 2006, The geological interpretation of well logs (second edition): Sutherland, Scotland, Whittles, 175 p.

Rowley, D.B., Forte, A.M., Moucha, R., Mitrovica, J.X., Simmons, N.A., and Grand, S.P., 2013, Dynamic topography change of the eastern United States since 3 million years ago: Science, doi:10.1126/science.1229180.

Sahagian, D., Pinous, O., Olferiev, A., Zakaharov, V., and Beisel, A., 1996, Eustatic curve for the Middle Jurassic–Cretaceous based on Russian platform and Siberian stratigraphy: Zonal resolution: American Association of Petroleum Geologists Bulletin, v. 80, p. 1433–1458.

Sheriff, R.E., 1985, Aspects of seismic resolution, *in* Berg, O.R., and Woolverton, E.G., eds., Seismic stratigraphy II—An integrated approach to hydrocarbon exploration: American Association of Petroleum Geologists Memoir 39, p. 1–10.

Thorne, J.A., and Watts, A.B., 1984, Seismic reflectors and unconformities at passive continental margins: Nature, v. 311, p. 365–368, doi:10.1038/311365a0.

Tucker, P., and Yorston, H., 1973, Pitfalls in seismic interpretation: Society of Exploration Geophysicists Monograph 2, 50 p., doi:10.1190/1.9781560802365.

Vail, P.R., Mitchum, R.M., Jr., Todd, R.G., Widmier, J.M., Thompson, S., III, Sangree, J.B., Bubb, J.N., and Hatlelid, W.G., 1977, Seismic stratigraphy and global changes of sea level, *in* Payton, C.E., ed., Seismic stratigraphy: Applications to hydrocarbon exploration: American Association of Petroleum Geologists Memoir 26, p. 49–212.

Vail, P.R., Mitchum, R.M., Jr., Shipley, T.H., and Buffler, R.T., 1980, Unconformities of the North Atlantic: Royal Society of London Philosophical Transactions, v. 294, p. 137–155, doi:10.1098/rsta.1980.0021.

Van Wagoner, J.C., Mitchum, R.M., Campion, K.M., and Rahmanian, V.D., 1990, Siliciclastic sequence stratigraphy in well logs, cores, and outcrops: Concepts for high-resolution correlation of time and facies: American Association of Petroleum Geologists Methods in Exploration Series 7, 55 p.

Widess, M.B., 1973, How thin is a thin bed?: Geophysics, v. 38, p. 1176–1180, doi:10.1190/1.1440403.